Submitted to Phys. Rev. C.

PUB-78-132-E
E-281

RECEIVED
MAY 8 1978 E81
DIRECTORS OFFICE
FERMILAB

Recoil properties of radionuclides formed in the interaction of 1-300 GeV protons with gold*

S. B. KAUFMAN, E. P. STEINBERG, and M. W. WEISFIELD[†]

Chemistry Division, Argonne National Laboratory
Argonne, Illinois 60439

The thick-target recoil properties of a number of nuclides, varying from ^{22}Na to ^{196}Au, formed in the interaction of 1-300 GeV protons with ^{197}Au have been measured in order to study the systematics of their variation with product mass and incident energy. The forward-to-backward ratios (F/B) of many of the products have a peak at 3 GeV and decrease at higher energies, with products in the mass region $46 \le A \le 65$ having F/B = 1.0 at 300 GeV. The F/B values of products with $A \gtrsim 140$ decrease monotonically between 1 and 300 GeV. The results are analyzed by the two-step model of high-energy reactions and discussed in terms of the different reaction mechanisms, spallation, fission

---

*Work performed under the auspices of the Division of Nuclear Physics of the Department of Energy.

[†] Present address: Radiation Management Corporation, Philadelphia, PA, 19104.

By acceptance of this article, the publisher and/or recipient acknowledges the U. S. Government's right to retain a non-exclusive, royalty-free license in and to any copyright covering this paper.

and fragmentation. Fission contributes appreciably to the formation of products in the mass region $46 \leq A \leq 103$ at 1 GeV bombarding energy, but other mechanisms predominate at and above 11.5 GeV. The results are compared to the predictions of intranuclear cascade-evaporation calculations, and are in reasonable agreement at 1 GeV and 3 GeV, although the calculations predict more forward momentum transfer than is observed. At higher energies the relation between forward momentum and mean deposition energy derived from the calculations must break down, because nuclides requiring high deposition energies for their formation have little or no forward momentum. Some possible explanations for this phenomenon are discussed.

[NUCLEAR REACTIONS ^{197}Au(p,x)^{22}Na - ^{196}Au, E_p = 1-300 GeV; measured thick-target recoil properties; derived momenta and deposition energies.]

I. INTRODUCTION

The interactions of high-energy protons with complex nuclei have been extensively studied by measurements of the recoil properties of the radionuclides formed in the reaction[1]. The thick-target, thick-catcher technique, in which both target and catchers are thick compared to the range of the products of interest, has been used extensively. Recoiling nuclei are collected in 2π geometry, and the fraction which recoil out of the target in the forward and backward directions with respect to the beam are measured. Often an auxiliary experiment is done to measure the fraction recoiling perpendicular to the beam. The analysis of the data is done using the two-step vector model of high-energy reactions, in a way first developed by Sugarman and coworkers[2-4]. The equations used in this analysis are further discussed by Winsberg and Alexander[1], and a more general treatment has recently been described by Winsberg[5].

In this model it is assumed that the velocity $\vec{v}_\ell$ of a recoil nuclide in the laboratory system is a sum of two vectors,

$$\vec{v}_\ell = \vec{v} + \vec{V} \ . \qquad (1)$$

The vector $\vec{v}$ results from the fast intranuclear cascade, and may be resolved into components parallel and perpendicular to the beam ($v_{||}$ and $v_{\perp}$). The vector $\vec{V}$ results from a slow second step of the reaction after the fast cascade (e.g., fission), and it is assumed that the two steps are sufficiently well separated in time so that memory of the beam direction, except for angular momentum effects, is lost. The angular distribution of $\vec{V}$ in the moving system will then be symmetric about 90° to the beam direction, on the average. Because of the integral nature of these thick-target, 2π experiments, other simplifying assumptions and approximations must be made in order to analyze the data. The distributions in $\vec{v}$ and $\vec{V}$ are assumed to be narrow and non-overlapping, with $\langle v \rangle \ll \langle V \rangle$, and the two vectors are assumed to be uncorrelated. Winsberg[5] has shown how an assumed distribution in $\vec{V}$ which may overlap $\langle v \rangle$ can be taken into account.

In order to test these assumptions for a particular type of reaction product it is necessary to make more detailed differential measurements of the angular distribution and energy spectra at different angles. In the case of products in the fission-fragment region formed from uranium by 2.2 GeV protons[6] it was found that the results were indeed consistent with the two-step model, and that the dominant process involved was binary fission after the fast cascade. The velocity $\vec{V}$ distributions were symmetric about 90°, and in fact were isotropic for the nuclides ^{103}Pd and ^{131}Ba, while that for ^{140}Ba was peaked at 90°. The distribution in magnitude of V was narrow for ^{140}Ba, and broader for the more neutron-deficient nuclides, particularly ^{131}Ba.

In another such study[7] angular and range measurements were made of ^{149}Tb formed from gold by 2.2 GeV protons, a product taken to be typical of "deep spallation", i.e., one far removed from the target nucleus and having an energy threshold of ca. 0.5 GeV. Again it was concluded that the data were consistent with the two-step model, provided a positive correlation between v and V was assumed. However, the two velocity distributions were found to be broad and overlapping, a condition which can lead to considerable errors in the analysis of thick-target data[8].

In the case of a third type of high-energy reaction, namely "fragmentation" (formation of light nuclei from heavy targets at GeV energies), the angular and energy distributions of ^{24}Na formed from bismuth at 2.9 GeV[9] could not be completely accounted for by a two-step process. There was no moving system in which both angular distributions and velocity spectra were symmetric about 90°; in order to achieve velocity symmetry the angular distribution must be forward-peaked, with a forward-to-backward ratio of 1.20. This indicates that there is no clear separation of the reaction into two steps, but that some memory of the beam direction is retained. However, when such light nuclides are formed from heavy targets at 28 GeV[10] the angular distributions tend to be peaked sidewards rather than forward, indicating a dramatic change in the nature of the interaction. Sideward peaking has recently been found[11] for products in the mass range 40-50 formed by 28 GeV protons incident on gold, and a change from forward to sideward peaking for copper isotopes from uranium was seen[12] when the proton energy was changed from 3 GeV to 11.5 GeV.

Although thick-target recoil experiments cannot test the assumptions of the model, they are extremely useful in carrying out broad surveys of the dependence on incident energy, target, and product mass. For example, thick-target measurements as a function of incident energy[13-15] have demonstrated a striking change in recoil properties occurring at about 3 GeV. At that energy, the forward-to-backward ratio (F/B) of certain nuclides goes through a maximum, after which it decreases with increasing energy up to 300 GeV. Both light fragments, such as ^{24}Na and ^{28}Mg formed from heavy targets[14] and Sc isotopes from uranium[15], as well as neutron-deficient nuclides in the middle-mass range from uranium[13] show this effect. In that same energy region, the ranges (and hence kinetic energies) of these neutron-deficient nuclides (e.g., ^{131}Ba) decrease by about a factor of two, also indicating a change in mechanism. The decreased F/B at higher incident energies is a consequence of the changes in angular distribution of light fragments from forward-peaked to sidewards-peaked[10-12].

In order to learn more about these changes in mechanism with bombarding energy we have made a survey of the thick-target recoil properties of a number of nuclides formed by the interaction of 1-300 GeV protons with gold. Much of the previous work in this field has been done using uranium as a target, and was concerned with the varying contributions of fission, fragmentation, and spallation mechanisms. The use of a relatively non-fissionable target, such as gold, tends to minimize the role of fission, although it will be seen that fission contributes to some extent, especially at 1 GeV proton energy.

In a previous paper[16] we have presented formation cross sections of a number of nuclides from gold bombarded with 11.5 and 300 GeV protons, using the technique of gross γ-ray spectroscopy to measure the different species. We have used the same technique in this work to measure the recoil properties of many of the same nuclides, thus permitting a systematic survey of how these properties vary with bombarding energy and product mass. In addition, chemical separations of osmium and gold from target and catchers were done at a single energy, 11.5 GeV, in order to extend the data to heavier masses.

II. EXPERIMENTAL PROCEDURE

The targets and catchers were irradiated with protons of 1.0-, 3.0-, and 11.5-GeV energy at the Argonne National Laboratory ZGS accelerator, 28.0-GeV energy at the Brookhaven National Laboratory AGS accelerator, and 300-GeV energy at the Fermilab (FNAL) accelerator. The 1.0- and 3.0-GeV irradiations were carried out in the internal circulating beam of the ZGS, while the 11.5-, 28.0-, and 300-GeV irradiations were done using external beams. At energies of 1.0-, 3.0-, and 28.0-GeV, two irradiations were done, while at 11.5- and 300-GeV four irradiations were done.

Targets for the external beams consisted of a gold foil, approximately 24 mg/cm^2 thick, sandwiched between Mylar catcher and guard foils of thickness 18 mg/cm^2. The foils in contact with the gold served as forward and backward catchers, and the others as activation blanks. The entire target stack was sealed in an evacuated polyethylene bag so that atmospheric pressure kept the foils in close contact. The foils were larger than the beam size, and after the irradiation an area containing the beam spot was cut out of the stack. Targets for the internal irradiations were similar, except that H-film catchers were used, and the leading edge and sides were cut before the irradiation to insure alignment of the different foils.

The target and catcher foils were counted without chemical separation using a Ge(Li) spectrometer to measure their γ-ray spectra over a period of time to follow the decay of the individual nuclidic γ-rays. The details of the determination of peak areas and the identification of individual nuclides by γ-ray energy and half-life have been given previously[16], along with a table of the γ-rays used in the measurements and the nuclide half-lives. The guard foils were included to determine the presence of any activities caused by impurities; the only such activities found were ^{22}Na and ^{24}Na, and the data for these two nuclides were corrected for the effect. The correction varied from 5% at 1.0 GeV to <0.2% at 11.5 GeV and above.

Of the nuclides whose cross sections were measured[16] by this technique, about half could be satisfactorily resolved in the spectra of the catchers, namely those nuclides whose mean range and cross section at a given bombarding energy are large enough to provide a sufficient activity level in the catchers. In order to extend the data to the low range products close to the target, several internal-beam irradiations were done at 11.5 GeV, and the elements osmium and gold chemically separated from target and catchers (which were aluminum foils in this case). Osmium was distilled as OsO_4 from acid solution, purified by a second distillation, and precipitated as the metal by reduction with Mg. Gold was extracted into ethyl acetate, purified by reduction to the metal followed by a second extraction, and precipitated as the metal.

III. RESULTS

The results of these measurements are the fractions of each nuclide which have recoiled out of a target of thickness W mg/cm^2 in the forward and backward direction, denoted by F and B, respectively. Rather than tabulating these quantities, two quantities more directly related to the parameters of interest are tabulated, namely the forward-to-backward ratio, F/B, and a quantity approximately equal to the mean range of the recoil in the target material, 2W(F + B). The experimental values of F/B at the five bombarding energies are given in Table I for each nuclide for which they were determined, and the values of 2W(F + B) are given in Table II. The latter values have all been corrected for scattering effects[17] at the target-catcher interface. The data for ^{24}Na and ^{28}Mg at energies of 11.5, 28.0, and 300 GeV are taken from ref. 14, but additional measurements at 1.0 and 3.0 GeV made since the previous work are reported here.

Some general features of the data can be seen directly. The F/B values represent in a sense the extent of forward peaking (in the beam direction) of the recoil, and thus are a measure of the forward momentum transferred to the target nucleus in the reaction which resulted in that recoil being formed. The variation of F/B with product mass at 11.5 GeV, the energy at which the most nuclides were measured, is shown in Fig. 1. Data in the literature for nuclides around A = 131 formed from gold at 11.5 GeV[18] and for Tb^{149} at the same energy[19] are included for comparison. Yu and Porile[18] found a significant variation of recoil properties with location on the charge dispersion curve, and since the present measurements at A > 130 include only nuclides representing the cumulative chain yield, only similar cases from ref. 18 are shown. The agreement between the present measurements and those of ref. 18 for $^{131}\mathrm{Ba}$ is good, as is that for $^{149}\mathrm{Gd}$ and the data of ref. 19 for $^{149}\mathrm{Tb}$ (the former is produced almost entirely by the electron-capture decay of the latter).

The general picture of how F/B varies with product mass, as revealed by Fig. 1, shows a rapid increase in forward peaking with increasing mass loss from the target (decreasing A) until about 20 amu have been lost (osmium isotopes). With further mass loss, going into the deep spallation region, the F/B values level off and then decrease. There is a broad minimum in the mass region A = 45-75, and then an increase as one goes to the light fragment region. A similar mass dependence has been observed previously[20,21] for the 19-GeV proton bombardment of tantalum.

The F/B values at 28.0 and 300 GeV are shown in Figs. 2a and 2b, again including data from the literature with the same target and bombarding energy[18,19,22]. For comparison with the more complete data at 11.5 GeV a smooth curve representing the trend at the latter energy is included. It can be seen from this comparison that the F/B values of all the nuclides measured here are smaller at the higher energies. At the highest energy, 300 GeV, the nuclides in the region of the minimum, A = 46-65, have values of F/B equal to unity, within experimental error. At 28 GeV these nuclides have F/B only slightly larger than unity. The implications of this behavior will be discussed in the following section. The recoil measurements of Cumming and Bächmann[22] at 28 GeV in the rare-earth region tend to lie somewhat below the present measurements, but the agreement is satisfactory. At 300 GeV the data of Yu and Porile[18] and Winsberg *et al.*[19] are also in general agreement with the present results.

The A-dependence of F/B at lower energies, 1.0 and 3.0 GeV, is shown in Fig. 3a and 3b, using a logarithmic scale because of the large range of values. Again, the smooth curves represent the trend of the 11.5-GeV data for comparison. The striking feature of these data is the large F/B values in the rare-earth region, where F/B $\gtrsim$ 10 at 1.0 GeV. It is also more apparent in Fig. 3 that there is not really a smooth variation with mass number, but that neighboring nuclides may have quite different recoil properties. In fact, as was observed for the A = 131 isobars[18], the recoil properties vary with the neutron-to-proton ratio, and that is apparent on comparing ^{58}Co and ^{59}Fe, for example, or ^{89}Zr and ^{90}Nb. The case of ^{103}Ru is noteworthy, having a much smaller F/B than the average trend, a fact connected with its location on the neutron-excess wing of the charge dispersion curve[16].

The variation of F/B with bombarding energy for specific nuclides is shown in Fig. 4. In Fig. 4a we show F/B for three of the lighter nuclides, ^{24}Na, ^{46}Sc, and ^{59}Fe. Additional data from the literature are included for ^{24}Na at 0.7 and 3.0 GeV[23] and at 6.0 and 200 GeV[14], and for ^{46}Sc and ^{59}Fe at 0.58 GeV[24]. Figure 4b shows data for the medium-mass nuclides ^{89}Zr, ^{90}Nb, and ^{103}Ru, including a measurement for ^{103}Ru at 0.58 GeV[24]. Figure 4c shows data for the heavy nuclides ^{131}Ba, ^{139}Ce, and ^{146}Gd, including a measurement for ^{131}Ba at 300 GeV[18].

The most striking feature of the curves in Fig. 4 is the presence of the peak in F/B at bombarding energies near 3 GeV. All of the light and medium-mass nuclides with the exception of ^{103}Ru exhibit this peak, and ^{131}Ba shows an indication of the peak. The heavier nuclides, in contrast, have F/B values that decrease monotonically above 1 GeV. This type of behavior was found previously[13] for isotopes of Sr and Ba formed from uranium, where the neutron-deficient nuclides showed a similar peaking, while the neutron-excess ones had F/B values close to unity and independent of bombarding energy. It appears that this peaking of the F/B near 3 GeV is a signature of high deposition energy processes, such as deep spallation and fragmentation.

In Fig. 4b one may also see the difference in the neighboring nuclides ^{89}Zr and ^{90}Nb, in that F/B is larger for the more neutron-deficient nuclide, ^{90}Nb. This increase of F/B in going toward the neutron-poor end of an isobaric chain was seen for the A = 131 isobars formed from gold at 11.5 GeV[18]. The relation between these thick-target F/B values and the true angular distribution is qualitative, but the present data indicates that angular distributions of almost all products formed from a heavy target will become less forward-peaked in the laboratory system above 3 GeV incident energy. Remsberg and Perry[10], for example, found that the angular distributions of light fragments (Na, Mg) were peaked sidewards at 28 GeV, in contrast to the forward peaking observed[9] at 2.9 GeV. Recent unpublished results[11,12] also confirm this.

The second recoil parameter, 2W(F + B), varies by nearly three orders of magnitude among the nuclides studied here. A general picture of how this quantity, which is essentially the mean recoil range, varies with product mass number is shown in Fig. 5 for the bombardments at 11.5 GeV. A logarithmic scale is used to encompass the large variation with mass number. The right-hand scale in Fig. 5 indicates the percentage loss from a target of 24 mg/cm^2 thickness. If less than about 1% of a nuclide recoils out of the target gross γ-ray spectroscopy cannot detect that nuclide in the catchers in the presence of the much greater levels of activity from higher-range nuclides, and chemical separations are necessary for the measurement.

A smooth curve has been drawn to indicate the trend of the data in Fig. 5, but once more it is clear that this is possible only because most of the nuclides measured by our technique tend to be those of largest cross section, and hence are the more neutron-poor nuclides. The three nuclides whose range deviates from the smooth trend, ^{59}Fe, ^{74}As, and ^{103}Ru, are neutron-rich relative to the peak of the charge-distribution curves[16], especially ^{103}Ru. Their relatively larger range is associated with a larger contribution of binary fission to their formation than for their more neutron-poor neighbors.

Inspection of Table II shows that the values of 2W(F + B) generally decrease with increasing bombarding energy. This effect is illustrated in Fig. 6, which shows the data at 1.0 GeV compared with the smooth curve representing the 11.5 GeV data. An examination of this energy dependence for individual nuclides is given in the following section, using the more meaningful quantity of kinetic energy derived from the range.

The measured recoil properties given in Tables I and II are related to the velocities v and V of the two-step model discussed in the Introduction. Under the assumptions given there, and if the range of a recoil in the target material, R_ℓ, can be related to its velocity by the expression

$$R_\ell = C\, v_\ell^{\;N} \qquad (2)$$

the following relationships have been derived:[1-4]

$$2W(F + B) = R_o \left\{ 1 + \left[\frac{\eta_{||}(N + 1)}{2} \right]^2 \right\} \tag{3}$$

$$\frac{F}{B} = \frac{1 + \frac{2}{3}\eta_{||}(N + 2) + \left[\frac{\eta_{||}(N + 1)}{2}\right]^2}{1 - \frac{2}{3}\eta_{||}(N + 2) + \left[\frac{\eta_{||}(N + 1)}{2}\right]^2} \tag{4}$$

$$\eta_{||} = \frac{v_{||}}{V} \tag{5}$$

In these equations R_o is the mean range in the target material corresponding via Eq. (2) to the velocity V, while $\eta_{||}$ is the ratio of the parallel component (in the beam direction) of the cascade velocity to the second-step velocity V. The perpendicular component of the cascade velocity, $v_{\perp}$, is assumed to be zero. Given an empirical range-velocity relation of the form of Eq. (2) these equations can be solved for the velocities v and V from the experimental data. It is also assumed that $\eta_{||} \ll 1$, so that terms of higher order than $\eta_{||}^2$ are neglected. For small $\eta_{||}$, Eq. (3) shows that the mean range $R_o = C\ V^N$ is slightly smaller than the quantity 2W(F + B).

For most nuclides the range-energy tables of Northcliffe and Schilling[25] were used to obtain values of C and N in Eq. (2). The average atomic number of each nuclide was calculated from the charge-dispersion curves derived[16] from the 11.5-GeV cross section data. Since the experimental ranges of the osmium and gold isotopes are less than the smallest value in the tables of ref. 25, the range-energy relation of Lindhard *et al.*[26] was used for these nuclides. For ^{22}Na, ^{24}Na, and ^{28}Mg the relationships derived by Winsberg[27] from experimental stopping powers were used.

The value of $\eta_{||}$ obtained from applying these equations to thick-target data is[1,5] approximately equal to $\langle Rv_{||}/V\rangle/\langle R\rangle$, because of the fact that the actual velocity distributions were assumed to be single-valued in the derivation. Winsberg[5] has presented a treatment which takes into account a distribution in V in order to estimate $\langle v_{||}/V\rangle$ from $\eta_{||}$. For the low-range products of $A > 130$ it is likely that the distributions of v and V are broad and overlapping, as in the case of ^{149}Tb formed from gold[7], and this effect can be significant.

In addition, correlations between $v_{||}$ and V have been inferred[7], which further complicates an estimation of $\langle v_{||}\rangle$ from $\langle v_{||}/V\rangle$. Since range is nearly proportional to kinetic energy for these low range recoils (N = 2 in Eq. (2)), one obtains the average kinetic energy, $\langle T\rangle$, from the mean range. On the other hand, range is more nearly proportional to velocity for the lighter products with relatively high kinetic energies, so that one obtains the average velocity $\langle V\rangle$, from the mean range. In the former case the best estimate of $v_{||}$ is given by

$$v_{||} = \langle v_{||}/V\rangle\langle V^2\rangle^{\frac{1}{2}} \quad , A > 130 \qquad (6)$$

and in the latter case by

$$v_{||} = \langle v_{||}/V\rangle\langle V\rangle \quad , A < 130 \qquad (7)$$

For products of A > 130 Cumming and Bächmann[22] have estimated that the values of $v_{||}$ obtained from Eq. (6) may be too large by as much as a factor of 1.4.

Calculations of the quantities V and $v_{||}$ were done both using Eqs. (2) to (7) and by the set of equations derived by Winsberg[5]. Comparison of the results of the two methods showed that the values of V were essentially identical, while the values of $v_{||}$ obtained by the latter method were higher than by the former method, but still within about 5%. The results given in Tables III and IV are those obtained using the method of Winsberg[5]. In Table III are given the mean momenta of the recoils, defined as $\langle P \rangle = A\langle V \rangle$, in units of $(\mathrm{MeV \cdot amu})^{\frac{1}{2}}$. We present the results in this way rather than directly as velocity V or kinetic energy $T = P^2/2A$, in order to facilitate comparison with binary fission. In addition this scales the data so that the small velocities of the heavy nuclides are more readily plotted as momenta. In Table IV are given values of the cascade velocity, $v_{||}$, in units of $(\mathrm{MeV/amu})^{\frac{1}{2}}$.

IV. DISCUSSION

A. *Kinetic energies and momenta*

The dependence of the mean kinetic energy of the recoiling nucleus on bombarding energy is shown in Fig. 7 for six "typical" nuclides, ^{24}Na, ^{54}Mn, ^{87}Y, ^{131}Ba, ^{149}Gd, and ^{167}Tm. The light fragmentation products, exemplified by ^{24}Na, exhibit a slowly decreasing kinetic energy as the bombarding energy increases. The magnitude of this energy, as has been pointed out before,[6,10,23] is comparable to that expected from the two-body breakup of a heavy excited nucleus. The decrease with increasing bombarding energy indicates that the average cascade residue leading to such light fragments becomes somewhat lighter at the higher energies, but the small extent of the decrease implies that there is no fundamental change in the process, although the formation cross sections increase by two orders of magnitude between 0.7 and 11.5 GeV[23].

Medium-mass nuclides, such as ^{54}Mn and ^{87}Y, have mean kinetic energies which are strongly dependent on bombarding energy, decreasing by about a factor of two between 1 and 11.5 GeV, with a further decrease above that energy. This behavior is quite similar to what is observed for many neutron-deficient medium-mass nuclides formed from uranium[13,14,28-33] and lead[34], where the change is characteristic of a change in mechanism from binary fission to deep spallation. In the case of gold as target the fission cross section is small, about 100 mb, and independent of energy above 1 GeV[35]. Cross sections for nuclides such as ^{54}Mn and ^{87}Y are rising rapidly[16] in this energy range, so it is not unexpected that the contribution of fission to their formation should decrease. Most of the nuclides between A = 46 and A = 96 behave very much the same, although ^{46}Sc has less of a decrease in kinetic energy between 1 and 11.5 GeV, and may have some contribution from a fragmentation mechanism. However, the very neutron-excess nuclide, ^{103}Ru, must still be formed mainly by fission even at 11.5 GeV, since its kinetic energy is essentially independent of bombarding energy. Its formation cross section is somewhat smaller at 11.5 GeV[16] than at 0.58 GeV[24] which is also in contrast with the increasing cross sections of the other nuclides.

The kinetic energy of ^{131}Ba decreases between 1 and 3 GeV by about 25% but then remains constant with bombarding energy. This can be interpreted as indicating some fission contribution to its formation at 1 GeV, but above 3 GeV such a contribution is small. Yu and Porile[18] have estimated on the basis of an analysis of both charge dispersion and recoil properties of the A = 131 isobars at 11.5 GeV that fission contributes ca. 2% of the isobaric yield. The kinetic energy of the heavier nuclides, such as ^{149}Gd and ^{167}Tm, are essentially independent of bombarding energy, as shown in Fig. 7. The thin-target measurement of Crespo *et al.*[7] on ^{149}Tb at 2.2 GeV is included for comparison with ^{149}Gd, showing the agreement. These nuclides available experimental data. Kotov *et al.*[39] have measured the kinetic energies of coincident fragments in the fission of gold by 1 GeV protons, using semiconductor detectors, and derived the mass distribution from them. The average fragment mass was 95 amu and the average total kinetic energy 126.5 MeV, and we have derived single-fragment mean kinetic energies from their data assuming a mean fissioning nucleus of A = 190. Because of momentum conservation, conversion to mean fragment momenta results in a curve symmetric about A = 95. We show in Fig. 9 this fission momentum curve along with the present recoil data at 1.0 GeV for comparison. The curve extends over the range of mass numbers where fission events were observed. We have included data for the osmium isotopes at 11.5 GeV in this figure, because we expect that their momenta should be the same at the lower energy, as suggested by Fig. 8.

The experimental momenta at 1.0 GeV for nuclides in the fission region are all significantly smaller than the momenta measured in the fragment coincidence experiment[39]. The reason for this is undoubtedly that in the latter experiment all events are of necessity binary fission, since a coincidence is required. In the present work, in contrast, all mechanisms forming a given nuclide are observed together; the non-fission events serve to lower the average momentum. For the set of nuclides from ^{46}Sc to ^{103}Ru (which we will refer to as medium-mass) at 1.0 GeV the ratio of experimental mean momentum to that expected for a are formed by a spallation-like mechanism, in which the second-step velocity V is the resultant of the many small recoils imparted by the evaporation of nucleons and heavier particles. There is essentially no change in this process with increasing bombarding energy, as indicated by the constancy of the mean kinetic energies.

The gold and osmium nuclides measured at 11.5 GeV are of some interest because they should be formed by a relatively simple spallation process, independent of bombarding energy above a few hundred MeV. This is shown in Fig. 8, where we compare the present data for these nuclides with data for the (p,pxn) products from bismuth at 0.45 GeV[36], to which the recoil analysis described above was applied to obtain mean momenta. It is clear that there is essentially no difference in the momenta of the ^{209}Bi(p,pxn) products at 0.45 GeV and those of the ^{197}Au(p,pxn) products at 11.5 GeV. The osmium isotopes, formed by more complex spallation reactions, have momenta at 11.5 GeV that are reasonable extrapolations of the low energy bismuth data.

We wish to compare the mean momenta with those expected from the different reaction mechanisms. In the case of fission one may use the liquid-drop theory[37] or fission systematics[38] to calculate the fragment energies given the Z, A, and nuclear temperature of the average fissioning nucleus. Since these are model dependent, we prefer in the present case to use some fission product lies in the range 0.62-0.78. There is no significant correlation of this quantity with neutron-to-proton ratio; for example, neutron-deficient ^{54}Mn has the same ratio, 0.78, as neutron-excess ^{103}Ru.

One may extend the fission curve to more asymmetric splits to estimate the momentum expected for ^{24}Na as a fission product as $P = 65$ (MeV·amu)$^{1/2}$; the ratio of the experimental momentum at 1 GeV to that value is 0.68, indicating that a fission-like (two-body) breakup mechanism may make a substantial contribution to light-fragment formation.

For the group of nuclides with $A > 130$, which we will refer to as the heavy-mass group, the experimental momenta are appreciably smaller, with ^{131}Ba and ^{139}Ce having ratios of 0.46 and 0.43 to the fission curve, respectively. The dashed curve in Fig. 9, labeled "spallation", was calculated using the cascade-evaporation model as follows. Two computer programs for the calculation of the initial intranuclear cascade were obtained and run on our computers: the VEGAS program[40,41] and the ORNL program[42]. The former is applicable up to 1 GeV incident energy, and the latter up to 3 GeV.

Although the models on which these two programs are based differ in some of their details, the fundamental assumptions are the same. The cascade is propagated by two-body interactions, classical trajectories are assumed, and the particles (including any pions produced) undergo further collisions independently.

The nuclear model represents the radial density distribution by a series of steps, but no clusters are included. These two models have been compared (along with a USSR program) at lower energies[43] and were found to yield similar results. We ran both programs for a total of 10,000 cascades for the case of 1.0 GeV protons incident on ^{197}Au. The results in terms of the distributions of excitation energy and momentum of the residual nuclei were the same within the statistical accuracy. The two sets of results were therefore combined for the succeeding evaporation calculation. For each cascade the identity, kinetic energy, and emission direction of each escaping particle was stored. From these the cascade velocity v and its components $v_{||}$ and $v_{\perp}$ could be calculated, as well as the atomic number, mass number, and excitation energy of the residual nucleus after each cascade.

The statistical evaporation of nucleons and clusters up to ^{4}He from the excited cascade residues was calculated by the Monte Carlo method described by Dostrovsky *et al.*[44] At each evaporation step the direction of particle emission was chosen at random, and the three components of recoil velocity summed with the resultants of the previous steps, in the same manner described by Porile and Tanaka[45]. In other words, particle evaporation was assumed isotropic in the system of the recoiling nucleus. The final velocity components were combined to give the second-step velocity V, which was then added vectorially to the cascade velocity v to obtain $\vec{v}_\ell$ [Eq. (1)]. To increase the statistical accuracy ten evaporations were done for each cascade residue.

These calculations yielded average values for a number of quantities of interest as a function of the final nuclide mass number. As expected[7], the distributions in the final velocities were quite broad, so that, for example, $<V^2>^{\frac{1}{2}} \approx 1.15<V>$ for most of the spallation products. Since the experimental mean momentum is $P = A <V^2>^{\frac{1}{2}}$, this is the quantity which was averaged and which is shown in Fig. 9 as the dashed curve labeled "spallation".

The experimental momenta are significantly larger than those calculated. This discrepancy has been noted by previous workers. For example, Crespo *et al.*[7] performed a similar evaporation calculation, using a single starting nucleus (^{186}Re) excited to 400, 500, and 600 MeV as a representative post-cascade nucleus in order to form ^{149}Tb. Comparing these results with the velocity distributions obtained from their differential thin-target measurements they found the same discrepancy, namely evaporation from stationary starting nuclei does not result in large enough recoil velocities. The data in Fig. 9 shows that this is true for a wide range of products. Similar discrepancies were found by Beg and Porile[13] and by Stark and Brandt[46]. This point will be discussed further after the mean momenta at higher bombarding energies are presented.

The mean momenta at 3.0 GeV are shown in Fig. 10a. In the medium-mass range the momenta are smaller than at 1.0 GeV, indicating less of a fission contribution at the higher energy. With the exception of ^{74}As and ^{103}Ru (solid points) they all have about the same momentum, ca. 60 $(\text{MeV}\cdot\text{amu})^{\frac{1}{2}}$. The spallation curve shown in Fig. 10a was calculated at 3.0 GeV using the ORNL intranuclear cascade program[42] in the same way as described above. Within statistics there is no difference between the calculations at 1.0 and 3.0 GeV, which is to be expected if the second (evaporation) step is independent of the first (cascade) step. Again, this calculated curve lies below the data points.

In Fig. 10b we show the mean momenta measured at 11.5 GeV. The medium-mass nuclides, except for ^{59}Fe, ^{74}As, and ^{103}Ru, all have nearly the same momentum, ca. 50 $(\text{MeV}\cdot\text{amu})^{\frac{1}{2}}$, smaller than at 3.0 GeV. The heavy-mass nuclides, as stated earlier, have momenta which are almost independent of bombarding energy. Although the available intranuclear cascade programs do not extend to such high incident energies, it is likely that the calculated momenta would again be appreciably smaller than those observed.

In going to still higher incident energies there is little further change in mean momenta. This is shown in Figs. 11a and 11b for 28 and 300 GeV, respectively, where the lines now indicate the average trend of the 11.5-GeV data for comparison. There are only small decreases of mean momenta at the higher incident energies. The neutron-excess nuclides ^{59}Fe and ^{74}As still tend to have larger momenta than their neighbors.

To summarize, we find that with increasing bombarding energy above 1 GeV most of the medium-mass nuclides are formed to an increasing extent by a mechanism which imparts considerably less momentum in the post-cascade step than does fission. This high-energy mechanism has been termed "deep spallation", that is, a spallation-like process leading to nuclides far removed from the target, and probably involving emission of light ($A \lesssim 20$) fragments, both on a time scale comparable with the cascade and afterwards, as in ordinary spallation. In contrast, the heavy nuclides have momenta which are independent of bombarding energy above 1 GeV, implying no change in mechanism. However, the momenta of these ordinary spallation products is larger than can be accounted for by evaporation of nucleons and clusters up to alpha particles. It is possible that inclusion of heavier evaporating particles in the calculation in an approximate way, such as by using enhanced statistical weights to simulate the various excited states[45], would provide better agreement. However, such evaporations should only be significant at high excitation energies, and would not affect the disagreement for near-spallation products such as the osmium isotopes.

Crespo *et al.*[7] suggested that the second-step velocity V as determined in a recoil experiment actually includes contributions from an "isotropic" part of the cascade velocity, arising from the broad distributions of $v_{||}$ and $v_{\perp}$. In other words, it may be that it is incorrect to identify the $\langle v_{||}\rangle$ as given by the intranuclear cascade calculations with the $\langle v_{||}\rangle$ of the two-step model.

This suggests that the cascade-evaporation calculation should be compared directly with the experimental data by calculating F/B and 2W(F + B). This was done for the cases of 1.0 and 3.0 GeV protons incident on gold in the manner described by Porile and Tanaka[45] and by Panontin *et al.*[47] At the conclusion of each evaporation case the kinetic energy of the recoil nucleus was converted to range, and a range-straggling dispersion[47] folded in. The range component along the beam direction was calculated from the recoil angle θ_L:

$$F_iW = R\cos\theta_L \quad (0 \leq \theta_L \leq \pi/2)$$

$$B_iW = -R\cos\theta_L \quad (\pi/2 \leq \theta_L \leq \pi) \tag{8}$$

At the end of the calculation the average recoil parameters were calculated for each mass number:

$$FW(A) = \frac{1}{N(A)}\sum F_iW$$

$$BW(A) = \frac{1}{N(A)}\sum B_iW \tag{9}$$

In this way, one does not attempt to separate the two steps of the process, but only considers the final result.

The results of this calculation for the spallation region ($\Delta A \lesssim 70$) are shown in Figs. 12 and 13. Fig. 12a shows the calculated values of 2W(F + B) at 1.0 GeV and the data at the same energy. The calculated results have been binned in 5 amu intervals to improve the statistics. The agreement with the data is good near A = 170, but the calculation predicts too large a range for the lighter masses. This is in contrast with the calculation shown in Fig. 9, where the calculated mean momenta due to the second step alone were smaller than the experimental values. In other words, the cascade part of the calculation does contribute to the isotropic part of the recoil velocity.

Figure 12b similarly shows the calculated values of 2W(F + B) at 3.0 GeV, together with the data at that energy and also the 11.5-GeV data for the osmium and gold isotopes. For $A > 188$ the calculated results are shown for each mass number, because of the rapid variation. The agreement at this energy is excellent for $A \gtrsim 140$, once again in contrast with the calculation of the second-step momenta without including the cascade contribution (Fig. 10a).

Unfortunately, such good agreement is not obtained when the calculated F/B values are compared with data, as shown in Figs. 13a and 13b. The calculation consistently overestimates the amount of forward peaking, especially for the deep spallation region, $A \lesssim 150$. In the next section this behavior is examined in more detail.

B. *Cascade velocities and excitation energy*

The mean cascade velocity in the beam direction, $\langle v_{||} \rangle$, obtained from the recoil data is given in Table IV for each nuclide at the different bombarding energies. The significance of this quantity is that intranuclear cascade calculations have shown a correlation between $\langle v_{||} \rangle$ and the average excitation energy, E*, of cascade residues. Using the results of an earlier intranuclear cascade calculation[48], Porile[49] found that the relation

$$\frac{E^*}{E_{CN}} = 0.8 \frac{\langle v_{||} \rangle}{v_{CN}} \qquad (10)$$

was satisfied for a variety of targets and bombarding energies up to 1.8 GeV. In Eq. (10) E_{CN} and v_{CN} are the excitation energy and velocity of the hypothetical compound nucleus formed in the reaction. This correlation was also found to hold for the more recent VEGAS model[40] up to 380 MeV. We have tested it for the VEGAS model[41] at 1.0 GeV and for the ORNL model[42] at 1.0 and 3.0 GeV, and the results are shown in Fig. 14. It is clear that Eq. (10) is valid for these cases also, and we will assume that if the models in their present form were extended to higher energies the relationship would still hold.

The mean cascade velocities as a function of nuclide mass for each incident energy from Table IV are shown in Figs. 15 and 16. The right-hand scale shows the excitation energy scale, calculated from Eq. (10). In Figs. 15a and 15b the dashed line shows the calculated values of $<v_{||}>$ as a function of A for the spallation products, from the cascade-evaporation calculations described above. At 1.0 GeV (Fig. 15a) the calculation predicts somewhat larger $<v_{||}>$ for ^{171}Lu and ^{167}Tm than is observed, but considerably overestimates the $<v_{||}>$ for the A = 131-149. This could be accounted for if binary fission played a significant role in the formation of these products, but the momenta do not support this hypothesis, as pointed out above. The nuclide ^{103}Ru, which is probably the only one shown which may be formed largely by fission, has the smallest $<v_{||}>$ of any.

For the medium-mass nuclides at 1.0 GeV the excitation energy increases as the mass number decreases, with ^{24}Na requiring the largest excitation energy for its formation. The general picture of the variation of E* with mass number shown in Fig. 15a is reasonable. The spallation products require more energy the further from the target they are, until fission, which can lead to large mass losses, starts to contribute. The formation of light fragments, as indicated also by their high energetic threshold, requires a large excitation energy for their formation.

At 3.0 GeV, as shown in Fig. 15b, the picture is nearly the same. The excitation energy for spallation products is smaller than demanded if they were formed only by evaporation of particles up to ^{4}He. The fission contribution to ^{131}Ba and ^{139}Ce has decreased, and their E* values have increased. Except for ^{103}Ru all of the medium-mass nuclides have larger E* values than at 1.0 GeV, also consistent with less fission contribution. Finally, the E* for ^{24}Na has doubled in going from 1.0 GeV to 3.0 GeV, consistent with its rapidly rising excitation function. Such a behavior is qualitatively consistent with estimates of E* based on excitation functions[50], and indicates the approximate validity of the relation between $\langle v_{||} \rangle$ and E* (Eq. (10)) up to 3 GeV.

However, at 11.5 GeV and above the relationship of Eq. (10) appears to break down, except for the near spallation products (e.g., the isotopes of gold and osmium). In Fig. 16 we show on an expanded scale the excitation energies for the gold and osmium isotopes, along with those of the ^{209}Bi(p,pxn) products at 0.45 GeV[36]. This comparison, as was also shown by the mean momenta (Fig. 8), indicates the independence of bombarding energy of the mechanism for forming these near-spallation products. The histogram is the calculated dependence of E* on ΔA at 3.0 GeV, and is in fairly good agreement with the data at both 0.45 GeV and 11.5 GeV.

We show the remainder of the 11.5 GeV data in Fig. 17a, where the dashed line represents the smooth trend of the calculated E* dependence on mass number for spallation. The discrepancy from the data for the deeper spallation products is serious; the derived excitation energy for these products is smaller at 11.5 GeV than at 3.0 GeV. This is the case for all the nuclides shown. Figs. 17b and 17c show that the derived excitation energy decreases further at higher incident energies, and that it becomes essentially zero for some of the medium-mass nuclides at 300 GeV. The variation of excitation energy with incident proton energy for some typical nuclides is shown in Fig. 18, which illustrates how E* decreases as the bombarding energy increases above 3 GeV.

The present study shows that for energies above about 3 GeV, a decrease in apparent E* [as calculated from $\langle v_{||} \rangle$ in Eq. (10)] with increasing incident energy is a general phenomenon, and not accounted for within the framework of existing theory. We shall examine some possible explanations for this behavior.

1. Forward Emission of Fragments. Alexander *et al.*[28] appear to have been the first to suggest that the emission of light nuclei, such as ^{24}Na, predominantly in the forward direction would tend to decrease the forward momentum component of the residual excited nucleus. This explanation was also put forth by others[7,13,15,18,22,23] in later papers. The force of this argument is reduced by the observation[10-12,14] that ^{24}Na itself, as well as other light nuclei, becomes less forward peaked at higher energies. Rather than causing the reduction in forward peaking for heavier nuclides, the light nuclei exhibit the same effect. However, very light nuclei ($Z \leq 8$) remain predominantly forward-peaked at 28 GeV[10], and may still be used

in this argument. The assumption is that if emission of clusters and light nuclei could be introduced into the intranuclear cascade calculations, a relationship between E* and $\langle v_{||} \rangle$ different than Eq. (10) would result.

An argument against this view is provided by the "coalescence" model[51,52] of formation of such light nuclei. This model, which has recently been successfully applied to relativistic heavy-ion reactions[53,54], assumes that among the cascade nucleons those with small relative momenta with respect to each other may coalesce to form a more complex particle. Under this model the momentum balance predicted by the conventional cascade calculations would not be affected by emission of complex particles, since the same nucleons with the same momenta would have been emitted anyway.

2. Emission of Excited Hadrons. Recent studies of hadron-nucleus collisions at multi-GeV energies[55] have shown that the time scales for particle production are large compared with nuclear transit times. Thus the projectile interacts with the nucleus as a single hadron after its first collision, and does not decay to its final multi-particle state until after it has left the nucleus. The multiplicity of charged particles emerging at small angles in a hadron-nucleus collision is independent of the nuclear mass[56,57], showing that these forward-traveling particles do not participate in the intranuclear cascade (i.e., there is no multiplication of particles).

Scheideman and Porile[15] suggested that the emission of such an excited hadron could account for the formation of residual nuclei with high excitation energy but low forward momentum. They considered a nucleon-nucleon collision inside the nucleus, with the projectile escaping as an excited hadron of mass m^*, and the target nucleon being captured by the nucleus, its kinetic energy becoming the nuclear excitation energy and its momentum the nuclear recoil momentum (the "Turkevich" model[58]). The relativistically correct equation applicable to this situation is[59]

$$m^{*2} = 1 + 2\, p_i q_{||} - 2\, T_R(E_i + 1) \tag{11}$$

where p_i and E_i are the momentum and total energy of the incident proton, and $q_{||}$ and T_R are the forward momentum component and kinetic energy of the recoiling target nucleon (assumed stationary initially). The units are $m_p = c = 1$. Replacing T_R by E^* and rearranging, we have

$$E^* = \frac{p_i q_{||}}{E_i + 1} - \frac{m^{*2} - 1}{2(E_i + 1)} \tag{12}$$

The first term in Eq. (12) has the same form as Eq. (10), since $p_i/(E_i + 1) = T_i/p_i \approx E_{CN}/p_{CN}$, only differing by the coefficient 0.8 in Eq. (10). The second term is zero for an elastic collision ($m^* = 1$), and causes E^* to decrease with increasing inelasticity. The effect of an inelastic collision is thus to decrease E^* for a given $q_{||}$, which is opposite to the desired effect. Therefore, it seems unlikely that such a process can account for the observed decrease in forward momentum.

3. Change in the Type of Excitons. The excitation energy may be thought of as residing in particle and hole excitons, formed as a result of the intranuclear cascade. The particle excitons are expected to contribute a net forward momentum while the holes should average out to zero momentum. If the excitons changed from predominantly particles below 3 GeV to predominantly holes above that energy, a decrease in forward momentum would result. This could occur if, for example, the target nucleons which are struck by the projectile tend to escape the nucleus more readily at high energy (perhaps as part of the forward "jet" of particles) instead of being captured.

4. Limiting Target Fragmentation. The limiting fragmentation concept, which was introduced by Benecke *et al.*[60] postulates that in an interaction of two hadrons the distribution of fragments of each hadron in its own rest frame becomes independent of energy in the limit of very high energies. This is shown, for example, by the distributions of pseudorapidity $\eta = -\ln(\frac{1}{2}\tan\theta_L)$ observed in proton-nucleus collisions above 50 GeV[57]. For small angles, $\eta > 4$, the charged-particle multiplicity is independent of target mass and in fact is the same as for pp interactions. This is termed the projectile fragmen-

tation region. At large angles, $\eta < 1$, the multiplicity is independent of incident energy, but increases with target mass as $A^{1/3}$. Thus in this target fragmentation region we expect the breakup of the target to be independent of the energy and nature of the projectile.

These concepts have been applied to relativistic heavy-ion reactions[61,62] where it was shown that the yields of nuclides from the fragmentation of copper with GeV protons and heavy ions were nearly identical. In this picture the target is a spectator whose breakup is nearly isotropic in its own rest frame, leading to the observed lack of forward peaking for many products.

Another way of describing this phenomenon is suggested by the "fireball" model proposed[54,63] for relativistic heavy-ion reactions. In this model the overlap between projectile and target forms a region where the nucleons are swept out, forming the fireball and leaving the non-overlapping regions of projectile and target as spectators with moderately low excitation. When the projectile is a proton we may picture it as drilling a hole through the nucleus, after which the remaining spectator portion breaks apart into two or more fragments. There is a considerable degree of momentum transfer to the fireball constituents, but relatively little to the spectator fragments.

V. SUMMARY

The dependence of recoil properties on incident energy and mass number of product has been studied for reactions of energetic protons with gold. The systematics of these data clearly illustrate the following features:

1. The variation of the F/B ratios with product mass is similar at all energies, having a broad minimum in the mass range A = 40-100. At the highest energy studied, 300 GeV, the F/B values in the minimum approach unity, indicating little or no forward momentum transfer from the projectile for events resulting in these products.

2. As a function of incident proton energy, F/B for many products rises between 1 and 3 GeV, then decreases at higher energies. This peak at 3 GeV is especially prominent for light and medium-mass nuclei for which the contribution of a specifically high-energy process (deep spallation) to their formation increases rapidly in this energy region. Nuclides formed mainly by fission, such as neutron-excess ^{103}Ru, exhibit energy-independent F/B values. Spallation products, within about 60-70 amu of the target, have monotonically decreasing F/B values with increasing energy.

3. The mean momenta of the recoiling nuclei at 1 GeV incident energy indicate a substantial fission contribution to the formation of products in the mass range A = 46-103. At

higher bombarding energies the momenta of the neutron-deficient products in this mass range decreases, showing that deep spallation, which results in smaller recoil momenta than fission, is becoming more prominent. The momenta of neutron-excess nuclides decreases by a smaller amount or not at all, depending on the proportions of fission and deep spallation which contribute to their formation. The mean momenta of the heavier nuclides ($A \geq 140$) are nearly independent of incident energy.

4. Comparison of the experimental data with the results of an intranuclear cascade - evaporation calculation shows that the mean momenta of all spallation products ($A > 130$) are larger than can be accounted for by evaporation of particles up to ^{4}He from stationary nuclei. However, if the cascade momentum is taken into account, the agreement is satisfactory. This suggests that the recoil analysis may not be able to completely separate the two steps of the reaction. Although the magnitude of the combined cascade and evaporation momenta are in agreement with the experimental ranges, the amount of forward peaking is overestimated by the calculation.

5. The relationship between deposition energy E^* and forward cascade velocity $v_{||}$ predicted by the model is at least qualitatively correct up to 3 GeV. At higher energies the relationship breaks down, with products which apparently require high deposition energies for their formation having little or no forward cascade velocity. Several possible explanations

for this change at relativistic energies are discussed, and although no firm conclusions can be drawn at this time, a process analagous to the nuclear fireball model proposed for relativistic heavy-ion reactions seems reasonable.

We wish to thank Dr. S. Katcoff for performing the bombardments at the AGS, and D. Henderson for assistance in counting the samples.

3/8/78 kek

TABLE I. Experimental values of the forward-to-backward ratio, F/B, of nuclides formed in the reactions of 1.0-, 3.0-, 11.5-, 28-, and 300-GeV protons with gold.

	Proton Energy (GeV)				
Nuclide	1.0	3.0	11.5	28.0	300
^{22}Na			1.60±0.06	1.37±0.07	1.30±0.07
^{24}Na	1.72±0.10	1.95±0.08	1.53±0.03	1.37±0.03	1.31±0.03
^{28}Mg		1.88±0.08	1.44±0.04	1.31±0.04	1.25±0.04
^{46}Sc	1.44±0.08	1.60±0.03	1.17±0.02	1.06±0.02	1.03±0.02
^{48}V		1.56±0.06	1.11±0.02	1.01±0.02	0.98±0.03
^{54}Mn	1.40±0.08	1.50±0.10	1.12±0.02	1.02±0.02	1.00±0.03
^{58}Co	1.60±0.06	1.54±0.07	1.10±0.03	1.04±0.03	0.99±0.03
^{59}Fe	1.32±0.05	1.40±0.05	1.12±0.03	1.01±0.04	1.04±0.03
^{65}Zn	1.43±0.08	1.50±0.06	1.12±0.03	1.01±0.04	1.00±0.03
^{74}As	1.34±0.05	1.40±0.05	1.16±0.02	1.06±0.04	1.10±0.03
^{75}Se		1.46±0.05	1.14±0.03	1.09±0.04	1.05±0.03
^{83}Rb	1.48±0.08	1.60±0.08	1.24±0.04	1.16±0.05	1.13±0.05
^{87}Y	1.42±0.04	1.67±0.05	1.26±0.02	1.19±0.03	1.15±0.03
^{89}Zr	1.43±0.05	1.67±0.03	1.28±0.03	1.18±0.03	1.17±0.03
^{90}Nb	1.63±0.06	1.81±0.08	1.35±0.04	1.18±0.06	1.21±0.04
^{96}Tc	1.45±0.05	1.76±0.07	1.32±0.03	1.30±0.07	1.32±0.06
^{103}Ru	1.27±0.08	1.27±0.10	1.25±0.10		
^{131}Ba	3.5 ± 0.2	3.8 ± 0.2	2.20±0.11		
^{139}Ce	5.2 ± 0.4	4.27±0.10	2.36±0.07	2.22±0.07	2.07±0.07
^{143}Pm			2.60±0.15		2.11±0.20
^{145}Eu	7.7 ± 0.5	4.36±0.18	2.60±0.18		2.19±0.15
^{146}Gd	7.8 ± 0.4	4.4 ± 0.2	2.65±0.15	2.48±0.10	2.25±0.10
^{149}Gd	8.6 ± 1.0	4.2 ± 0.2	2.75±0.10	2.49±0.10	2.21±0.11
^{167}Tm	9.2 ± 0.6	3.8 ± 0.4	2.6 ± 0.2		
^{171}Lu	8.0 ± 0.5	3.4 ± 0.2	2.7 ± 0.2		
^{182}Os			3.01±0.04		
^{183}Os			2.94±0.11		
^{183}Os^{m}			3.09±0.13		
^{185}Os			2.80±0.20		
^{194}Au			2.18±0.03		
^{196}Au			1.51±0.04		

TABLE II. Experimental recoil ranges [2W(F + B)] of nuclides formed in the reactions of 1.0-, 3.0-, 11.5-, 28.0-, and 300-GeV protons with gold. The units are mg/cm^2, and the data have been corrected for scattering as described in the text.

	Proton Energy (GeV)				
Nuclide	1.0	3.0	11.5	28.0	300
^{22}Na			14.8±0.6	13.8±0.8	13.8±0.7
^{24}Na	12.6±1.0	14.8±0.8	12.7±0.4	11.8±0.4	11.8±0.4
^{28}Mg		17.8±1.0	14.2±0.4	13.2±0.5	13.2±0.4
^{46}Sc	10.0±0.8	8.6±0.6	7.32±0.15	6.92±0.10	6.75±0.15
^{48}V		9.7±0.5	6.94±0.20	6.47±0.22	6.39±0.20
^{54}Mn	10.4±0.8	8.1±0.3	6.46±0.22	6.18±0.17	6.02±0.23
^{58}Co	9.1±1.5	7.7±0.4	6.18±0.33	5.95±0.26	5.98±0.20
^{59}Fe	9.9±0.5	8.4±0.4	6.94±0.30	6.71±0.24	6.52±0.26
^{65}Zn	8.4±0.6	6.7±1.1	5.51±0.24	5.18±0.20	5.24±0.20
^{74}As	8.8±0.4	8.1±0.4	6.22±0.16	5.91±0.15	5.61±0.30
^{75}Se		6.3±0.4	4.94±0.15	4.88±0.17	4.66±0.19
^{83}Rb	6.7±0.7	5.4±0.3	4.47±0.20	4.30±0.15	4.21±0.20
^{87}Y	7.2±0.4	5.33±0.20	4.38±0.16	4.09±0.14	4.04±0.05
^{89}Zr	7.6±0.4	5.33±0.22	4.10±0.15	4.22±0.25	3.97±0.03
^{90}Nb	6.0±0.6	4.8±0.6	4.05±0.25	3.57±0.27	3.57±0.10
^{96}Tc	7.4±0.6	4.8±0.5	3.82±0.17	3.87±0.15	3.89±0.15
^{103}Ru	7.4±0.8	6.3±1.0	7.1±0.7		
^{131}Ba	2.37±0.15	1.92±0.05	1.71±0.10		
^{139}Ce	1.79±0.14	1.55±0.03	1.33±0.07	1.28±0.03	1.24±0.05
^{143}Pm			1.22±0.06		1.20±0.05
^{145}Eu	1.49±0.12	1.28±0.03	1.19±0.04		1.12±0.02
^{146}Gd	1.43±0.15	1.23±0.03	1.12±0.03	1.09±0.03	1.02±0.07
^{149}Gd	1.33±0.10	1.17±0.03	1.02±0.05	1.00±0.03	0.90±0.06
^{167}Tm	0.71±0.06	0.59±0.02	0.54±0.03		
^{171}Lu	0.60±0.05	0.53±0.02	0.51±0.03		
^{182}Os			0.215±0.010		
^{183}Os			0.200±0.009		
^{183}Os^{m}			0.198±0.010		
^{185}Os			0.169±0.010		
^{194}Au			0.061±0.006		
^{196}Au			0.030±0.002		

TABLE III. The mean momentum <P> = A<V> after the cascade of nuclides formed in the reactions of 1.0-, 3.0-, 11.5-, 28-, and 300 GeV protons with gold. The units are (MeV·amu)$^{1/2}$.

	Proton Energy (GeV)				
Nuclide	1.0	3.0	11.5	28.0	300
^{22}Na			45.8±1.2	44.4±1.6	44.5±1.4
^{24}Na	44.0±2.2	47.4±1.7	44.4±1.0	42.9±1.0	43.0±1.0
^{28}Mg		59.3±2.2	52.4±1.0	50.3±1.2	50.4±1.0
^{46}Sc	62.1±4.3	54.3±3.5	47.5±0.9	45.0±1.2	44.7±0.9
^{48}V		65.5±3.1	48.8±1.3	45.7±1.4	45.1±1.3
^{54}Mn	74.4±5.1	59.3±2.0	48.7±1.4	47.5±1.1	46.0±1.6
^{58}Co	70.4±10.4	60.6±2.9	49.7±2.2	48.6±1.9	48.3±1.5
^{59}Fe	74.3±3.5	63.4±2.8	53.7±2.2	51.9±1.8	51.4±1.9
^{65}Zn	71.0±4.6	58.4±8.6	49.3±1.7	46.3±1.6	46.7±1.6
^{74}As	81.1±3.5	74.3±3.4	58.8±1.3	56.1±1.3	54.1±2.7
^{75}Se		60.4±3.3	49.9±1.3	49.4±1.3	47.4±1.7
^{83}Rb	68.3±5.7	57.5±2.6	49.4±1.8	47.9±1.3	47.2±1.8
^{87}Y	74.7±3.3	58.8±1.7	50.6±1.4	47.9±1.4	47.4±0.5
^{89}Zr	78.8±3.2	60.1±1.8	49.2±1.4	50.5±2.3	48.1±0.3
^{90}Nb	66.3±5.0	55.5±5.3	49.7±2.3	45.1±2.4	45.1±1.0
^{96}Tc	83.9±6.3	57.5±4.3	49.4±1.4	49.8±1.4	50.0±1.4
^{103}Ru	85.5±9.0	73.6±11.3	79.0±7.9		
^{131}Ba	46.2±1.6	40.9±0.6	40.4±1.3		
^{139}Ce	40.2±1.7	38.1±0.4	37.1±1.0	36.6±0.4	36.1±0.8
^{143}Pm			36.5±0.8		36.8±0.8
^{145}Eu	36.6±1.2	36.3±0.4	36.6±0.6		36.0±0.3
^{146}Gd	36.1±1.9	35.9±0.4	35.8±0.5	35.6±0.5	34.7±1.2
^{149}Gd	35.0±1.3	35.6±0.5	34.7±0.9	34.6±0.5	33.0±1.1
^{167}Tm	29.1±1.3	29.4±0.5	29.1±0.8		
^{171}Lu	27.9±1.2	28.9±0.6	29.0±0.9		
^{182}Os			17.6±0.4		
^{183}Os + ^{183}Os^{m}			16.9±0.5		
^{185}Os			15.5±0.6		
^{194}Au			9.3±0.6		
^{196}Au			5.84±0.27		

TABLE IV. The cascade velocity, $\langle v_{||} \rangle$, of nuclides formed in the reactions of 1.0-, 3.0-, 11.5-, 28-, and 300-GeV protons with gold. The units are $(\mathrm{MeV/amu})^{1/2}$.

	Proton Energy (GeV)				
Nuclide	1.0	3.0	11.5	28.0	300
^{22}Na			0.183±0.016	0.119±0.020	0.100±0.021
^{24}Na	0.186±0.024	0.247±0.019	0.148±0.008	0.106±0.008	0.091±0.008
^{28}Mg		0.270±0.023	0.138±0.011	0.098±0.012	0.081±0.012
^{46}Sc	0.116±0.021	0.133±0.013	0.039±0.004	0.014±0.005	0.007±0.005
^{48}V		0.147±0.016	0.026±0.004	0.002±0.003	0.0 ±0.007
^{54}Mn	0.111±0.022	0.108±0.018	0.025±0.004	0.004±0.004	0.0 ±0.007
^{58}Co	0.136±0.031	0.109±0.014	0.020±0.006	0.008±0.006	0.0 ±0.006
^{59}Fe	0.085±0.013	0.088±0.011	0.025±0.006	0.002±0.005	0.008±0.006
^{65}Zn	0.094±0.017	0.088±0.020	0.021±0.005	0.002±0.004	0.0 ±0.006
^{74}As	0.079±0.011	0.082±0.010	0.029±0.003	0.011±0.007	0.017±0.005
^{75}Se		0.072±0.009	0.021±0.004	0.013±0.006	0.007±0.004
^{83}Rb	0.074±0.013	0.074±0.009	0.029±0.005	0.020±0.006	0.016±0.006
^{87}Y	0.069±0.007	0.079±0.006	0.032±0.002	0.022±0.003	0.018±0.003
^{89}Zr	0.072±0.008	0.078±0.004	0.031±0.003	0.021±0.004	0.019±0.003
^{90}Nb	0.081±0.011	0.082±0.013	0.037±0.004	0.019±0.006	0.022±0.004
^{96}Tc	0.079±0.011	0.075±0.010	0.032±0.003	0.030±0.006	0.032±0.005
^{103}Ru	0.049±0.015	0.042±0.017	0.042±0.016		
^{131}Ba	0.089±0.006	0.084±0.004	0.049±0.003		
^{139}Ce	0.095±0.007	0.079±0.002	0.046±0.002	0.042±0.002	0.038±0.002
^{143}Pm			0.049±0.003		0.038±0.005
^{145}Eu	0.101±0.006	0.073±0.003	0.048±0.004		0.039±0.003
^{146}Gd	0.100±0.008	0.072±0.003	0.048±0.003	0.044±0.002	0.038±0.003
^{149}Gd	0.099±0.008	0.068±0.003	0.047±0.002	0.042±0.002	0.035±0.002
^{167}Tm	0.076±0.005	0.047±0.004	0.033±0.003		
^{171}Lu	0.067±0.005	0.041±0.002	0.033±0.003		
^{182}Os			0.022±0.001		
^{183}Os + ^{183}Os^{m}			0.021±0.001		
^{185}Os			0.018±0.002		
^{194}Au			$(7.9\pm0.6)\cdot10^{-3}$		
^{196}Au			$(2.7\pm0.3)\cdot10^{-3}$		

References

1. For a general review, see J. M. Alexander, in *Nuclear Chemistry*, edited by L. Yaffe (Academic, New York, 1968), Vol. I, p. 273; L. Winsberg and J. M. Alexander, ibid, p. 340.
2. N. Sugarman, M. Campos, and K. Wielgoz, Phys. Rev. 101, 388 (1956).
3. N. T. Porile and N. Sugarman, Phys. Rev. 107, 1410 (1957).
4. N. Sugarman, H. Münzel, J. A. Panontin, K. Wielgoz, M. V. Ramaniah, G. Lange, and E. Lopez-Menchero, Phys. Rev. 143, 952 (1966).
5. L. Winsberg, Nuclear Instr. Meth., to be published.
6. V. P. Crespo, J. B. Cumming, and A. M. Poskanzer, Phys. Rev. 174, 1455 (1968).
7. V. P. Crespo, J. B. Cumming, and J. M. Alexander, Phys. Rev. C2, 1777 (1970).
8. N. T. Porile, Phys. Rev. 185, 1371 (1969).
9. J. B. Cumming, R. J. Cross, Jr., J. Hudis, and A. M. Poskanzer, Phys. Rev. 134, B167 (1964).
10. L. P. Remsberg and D. G. Perry, Phys. Rev. Lett. 35, 361 (1975).
11. R. L. Klobuchar, J. B. Cumming, and G. J. Virtes, 174th Meeting of the American Chemical Society, Chicago, Illinois, September, 1977, paper NUCL-72.

12. J. A. Urbon, E. P. Steinberg, and S. B. Kaufman, 174th Meeting of the American Chemical Society, Chicago, Illinois, September, 1977, paper NUCL-78.

13. K. Beg and N. T. Porile, Phys. Rev. C3, 1631 (1971).

14. S. B. Kaufman and M. W. Weisfield, Phys. Rev. C11, 1258 (1975).

15. Ø. Scheidemann and N. T. Porile, Phys. Rev. C14, 1534 (1976).

16. S. B. Kaufman, M. W. Weisfield, E. P. Steinberg, B. D. Wilkins, and D. Henderson, Phys. Rev. C14, 1121 (1976).

17. J. A. Panontin and N. Sugarman, J. Inorg. Nucl. Chem. 25, 1321 (1963).

18. Y. W. Yu and N. T. Porile, Phys. Rev. C12, 938 (1975).

19. L. Winsberg, M. W. Weisfield, and D. Henderson, Phys. Rev. C13, 279 (1976).

20. B. Neidhart and K. Bächmann, J. Inorg. Nucl. Chem. 34, 423 (1972).

21. K. Bächmann, B. Neidhart, and E. Ross, Radiochimica Acta 18, 133 (1972).

22. J. B. Cumming and K. Bächmann, Phys. Rev. C6, 1362 (1972).

23. V. P. Crespo, J. M. Alexander, and E. K. Hyde, Phys. Rev. 131, 1765 (1963).

24. E. Ross and K. Bächmann, Radiochimica Acta 21, 13 (1974).

25. L. C. Northcliffe and R. F. Schilling, Nucl. Data A7, 233 (1970).

26. J. Lindhard, M. Scharff, and H. E. Schiøtt, Kgl. Danske Videnskab. Selskab, Mat.-Fys. Medd. 33, No. 14 (1963).

27. L. Winsberg, Atomic Data Tables (to be published).

28. J. M. Alexander, C. Baltzinger, and M. F. Gazdik, Phys. Rev. 129, 1826 (1963).

29. E. Hagebø and H. Ravn, J. Inorg. Nucl. Chem. 31, 2649 (1969).

30. J. A. Panontin and N. T. Porile, J. Inorg. Nucl. Chem. 32, 1775 (1970).

31. R. Brandt, Radiochim. Acta 16, 148 (1971).

32. P. M. Starzyk and N. Sugarman, Phys. Rev. C8, 1448 (1973).

33. S. K. Chang and N. Sugarman, Phys. Rev. C8, 775 (1973).

34. J. A. Panontin and N. T. Porile, J. Inorg. Nucl. Chem. 33, 3211 (1971).

35. J. Hudis and S. Katcoff, Phys. Rev. C13, 1961 (1976).

36. W. R. Pierson and N. Sugarman, Phys. Rev. 130, 2417 (1963).

37. J. R. Nix and W. J. Swiatecki, Nucl. Phys. 71, 1 (1965).

38. V. E. Viola, Jr., Nucl. Data A1, 391 (1966).

39. A. A. Kotov, G. G. Semenchuck, L. N. Andronenko, M. N. Andronenko, B. L. Gorshkov, G. G. Kovshevnyi, V. R. Reznik, and G. E. Solyakin, Sov. J. Nucl. Phys. 20, 251 (1975).

40. K. Chen, Z. Fraenkel, G. Friedlander, J. R. Grover, J. M. Miller, and Y. Shimamoto Phys. Rev. 166, 949 (1968).

41. G. D. Harp, Phys. Rev. C10, 2387 (1974).

42. H. W. Bertini, Phys. Rev. C6, 631 (1972).

43. V. S. Barashenkov, H. W. Bertini, K. Chen, G. Friedlander, G. D. Harp, A. S. Iljinov, J. M. Miller, and V. D. Toneev, Nucl. Phys. A187, 531 (1972).

44. I. Dostrovsky, Z. Fraenkel, and G. Friedlander, Phys. Rev. 116, 683 (1959).

45. N. T. Porile and S. Tanaka, Phys. Rev. 135, B122 (1964).

46. G. Stark and R. Brandt, Radiochim. Acta 16, 155 (1971).

47. J. A. Panontin, N. T. Porile, and A. A. Caretto, Jr., Phys. Rev. 165, 1281 (1968).

48. N. Metropolis, R. Bivins, M. Storm, A. Turkevich, J. M. Miller, and G. Friedlander, Phys. Rev. 110, 185 (1958).

49. N. T. Porile, Phys. Rev. 120, 572 (1960).

50. N. T. Porile and N. Sugarman, Phys. Rev. 107, 1422 (1957).

51. S. T. Butler and C. A. Pearson, Phys. Rev. Lett. 7, 69 (1961); Phys. Rev. 129, 836 (1963).

52. A. Schwarzschild and C. Zupancic, Phys. Rev. 129, 854 (1963).

53. H. H. Gutbrod, A. Sandoval, P. J. Johansen, A. M. Poskanzer, J. Gosset, W. G. Meyer, G. D. Westfall, and R. Stock, Phys. Rev. Lett. 37, 667 (1976).

54. J. Gosset, H. H. Gutbrod, W. G. Meyer, A. M. Poskanzer, A. Sandoval, R. Stock, and G. D. Westfall, Phys. Rev. C16, 629 (1977).

55. For a review of this subject, see W. Busza, in *High-Energy Physics and Nuclear Structure - 1975* (American Institute of Physics, New York, 1975), p. 211.

56. W. Busza, J. E. Elias, D. F. Jacobs, P. A. Swartz, C. C. Young, and M. R. Sogard, Phys. Rev. Lett. 34, 836 (1975).

57. C. Halliwell, J. E. Elias, W. Busza, D. Luckey, L. Votta, and C. Young, Phys. Rev. Lett. 39, 1499 (1977).

58. A. Turkevich, quoted in N. T. Porile and N. Sugarman, Phys. Rev. 107, 1410 (1957).

59. A. M. Poskanzer, J. B. Cumming, and L. P. Remsberg, Phys. Rev. 168, 1331 (1968).

60. J. Benecke, T. T. Chou, C. N. Yang, and E. Yen, Phys. Rev. 188, 2159 (1969).

61. J. B. Cumming, P. E. Haustein, R. W. Stoenner, L. Mausner, and R. A. Naumann, Phys. Rev. C10, 739 (1974).

62. J. B. Cumming, R. W. Stoenner, and P. E. Haustein, Phys. Rev. C14, 1554 (1976).

63. G. D. Westfall, J. Gosset, P. J. Johansen, A. M. Poskanzer, W. G. Meyer, H. H. Gutbrod, A. Sandoval, and R. Stock, Phys. Rev. Lett. 37, 1202 (1976).

Figure Captions

Fig. 1. The dependence of the forward-to-backward ratio, F/B, on mass number at 11.5 GeV. □, Ref. 18; Δ, Ref. 19.

Fig. 2. The dependence of F/B on mass number at 28 GeV (a) and 300 GeV (b) . ∇, Ref. 22; □, Ref. 18; Δ, Ref. 19. The curve shows the general trend of F/B at 11.5 GeV from Fig. 1.

Fig. 3. The dependence of F/B on mass number at 1.0 GeV (a) and 3.0 GeV (b). Δ, Ref. 19. The curve shows the general trend of F/B at 11.5 GeV.

Fig. 4. The variation of F/B with incident proton energy for some typical nuclides. Some of the points have been displaced slightly in energy for clarity. The curves are to guide the eye.

Fig. 5. The dependence of the mean range, 2W(F + B), on mass number at 11.5 GeV. The right-hand scale gives the percentage recoil loss from a 24 mg/cm^2 target. □, Ref. 18; Δ, Ref. 19. The curve is to show the trend of the data.

Fig. 6. The dependence of 2W(F + B) on mass number at 1.0 GeV. Δ , Ref. 19. The curve shows the trend of 2W(F + B) at 11.5 GeV from Fig. 5.

Fig. 7. The variation of mean kinetic energy, <T>, with incident proton energy for some typical nuclides. The curves are drawn to guide the eye. The point (▼) at 2.2 GeV is from the thin-target measurements of Ref. 7 on ^{149}Tb.

Fig. 8. Mean momenta as a function of mass difference from the target, ΔA. ○, present data at 11.5 GeV; Δ data of Ref. 36 for bismuth target at 0.45 GeV.

Fig. 9. The dependence of the mean momentum on mass number at 1.0 GeV. The solid curve shows the momentum for binary fission (see text) and the dashed curve the calculated momenta for spallation (see text). ●, data at 11.5 GeV; Δ, Ref. 19.

Fig. 10. The dependence of the mean momenta on mass number at 3.0 GeV (a) and 11.5 GeV (b). The solid curves are for fission at 1.0 GeV, and the dashed curve is the spallation calculation at 3.0 GeV (see text). ●, neutron-excess nuclides, ^{59}Fe, ^{74}As, ^{103}Ru; Δ, Ref. 19; □, Ref. 18; ◇, Ref. 23.

Fig. 11. The dependence of the mean momenta on mass number at 28 GeV (a) and 300 GeV (b). The two curves show the trend of the 11.5-GeV data for comparison. ●, neutron-excess nuclides, ^{59}Fe, ^{74}As; ▽, Ref. 22; □, Ref. 18; Δ, Ref. 19.

Fig. 12. Calculated and experimental values of 2W(F + B) at 1.0 GeV (a) and 3.0 GeV (b). ●, data at 11.5 GeV; Δ, Ref. 19.

Fig. 13. Calculated and experimental values of F/B at 1.0 GeV (a) and 3.0 GeV (b). ●, data at 11.5 GeV; Δ, Ref. 19.

Fig. 14. Correlation between forward velocity component and excitation energy of cascade products, both relative to the maximum (CN) values, for protons incident on ^{197}Au. O, VEGAS calculation, 1.0 GeV; X, ORNL calculation, 1.0 GeV; +, ORNL calculation, 3.0 GeV. The line is Eq. (10).

Fig. 15. Mean cascade velocity $\langle v_{||} \rangle$ and derived deposition energy E* at 1.0 GeV (a) and 3.0 GeV (b). The dashed lines are the results of the cascade-evaporation calculations.

Fig. 16. Calculated deposition energies as a function of mass difference from the target, ΔA. O, present data at 11.5 GeV; Δ, data of Ref. 36 for bismuth target at 0.45 GeV.

Fig. 17. Mean cascade velocity $\langle v_{||} \rangle$ and derived deposition energy E* at 11.5 GeV (a), 28 GeV (b), and 300 GeV (c). The dashed line shows the calculated (at 3.0 GeV) variation of E* with mass number.

Fig. 18. Variation of E* with incident proton energy for some typical nuclides. The lines merely connect points to guide the eye. Data for ^{24}Na at 0.7 GeV from Ref. 23, at 6 and 200 GeV from Ref. 14.

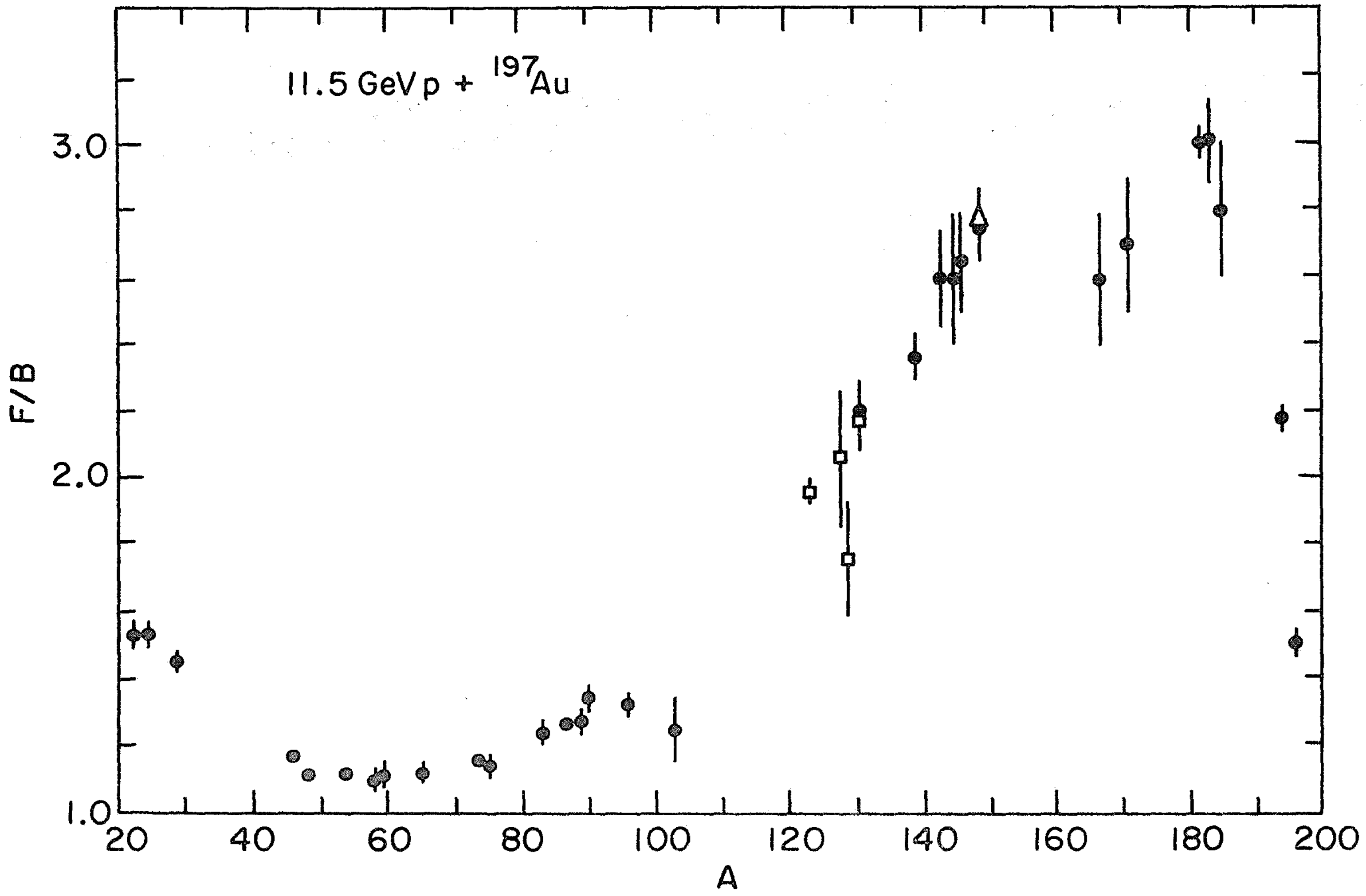
11.5 GeV p + ^{197}Au
F/B
1.0
2.0
3.0
A
20
40
60
80
100
120
140
160
180
200

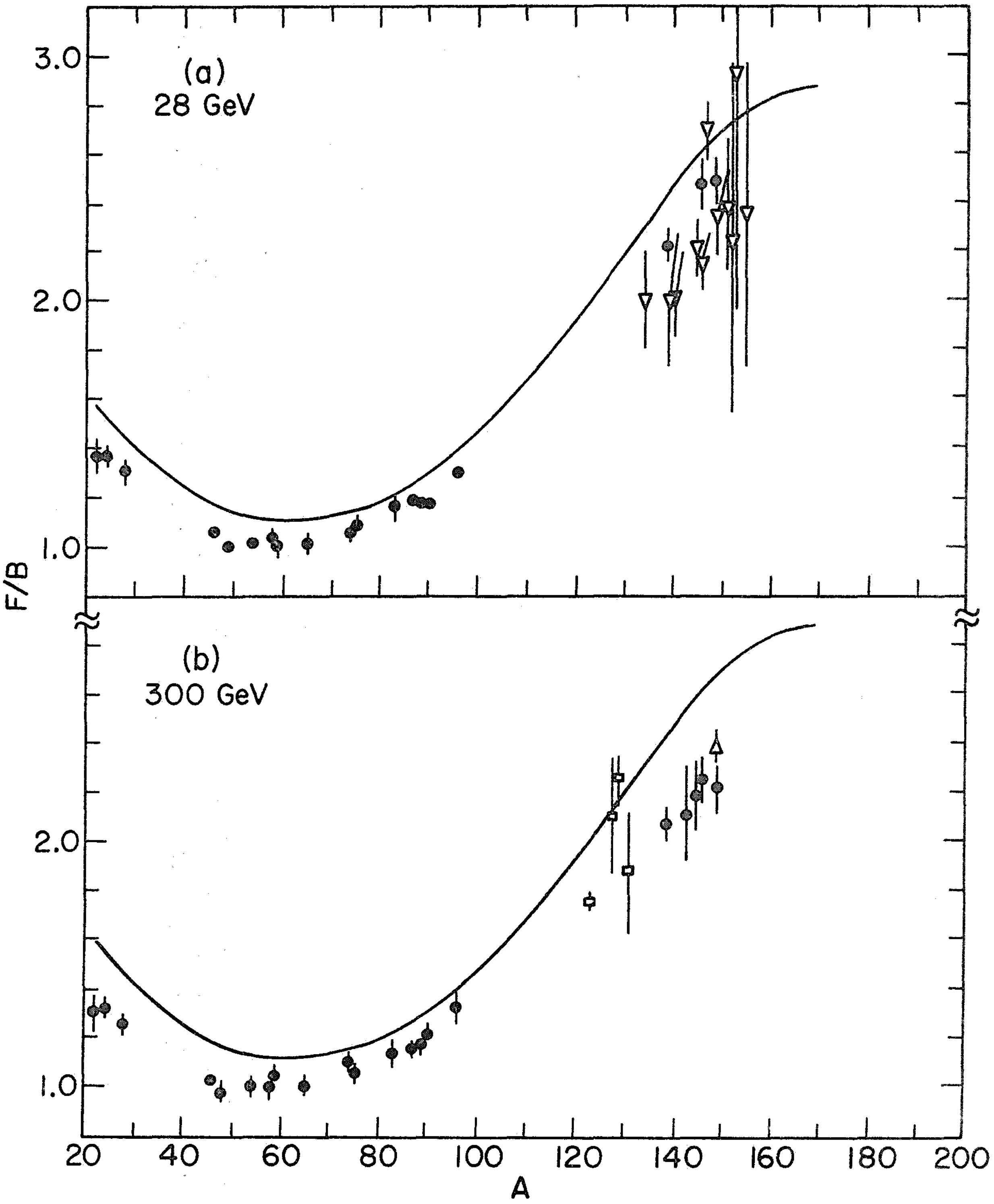
(a)
28 GeV
3.0
2.0
1.0
F/B
(b)
300 GeV
2.0
1.0
20
40
60
80
100
120
140
160
180
200
A

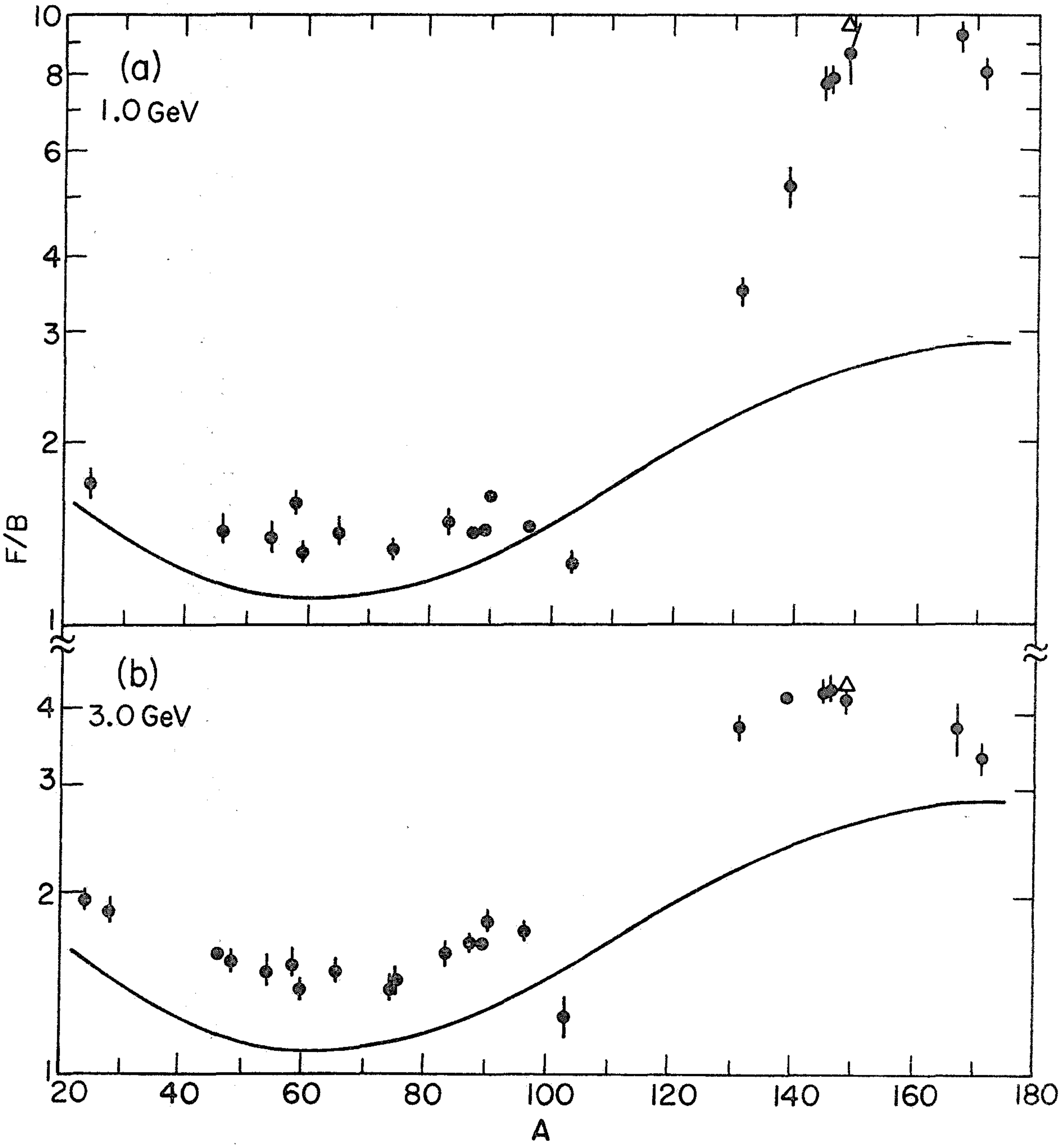
(a)
1.0 GeV
(b)
3.0 GeV
F/B
A
10
8
6
4
3
2
1
4
3
2
1
20
40
60
80
100
120
140
160
180

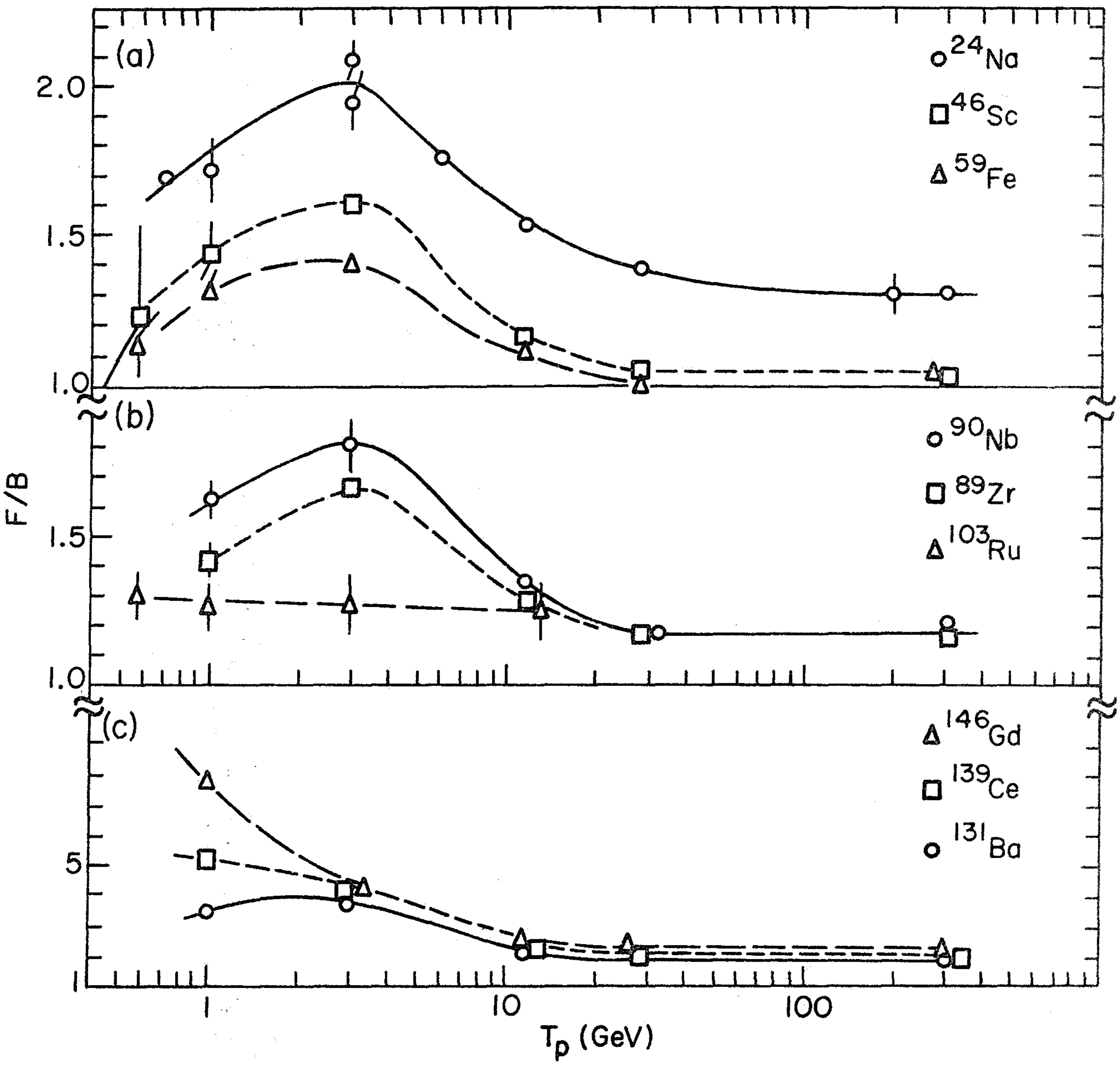
(a)
2.0
1.5
1.0
○ ^{24}Na
□ ^{46}Sc
Δ ^{59}Fe
(b)
F/B
1.5
1.0
○ ^{90}Nb
□ ^{89}Zr
Δ ^{103}Ru
(c)
5
1
Δ ^{146}Gd
□ ^{139}Ce
○ ^{131}Ba
1
10
100
T_p (GeV)

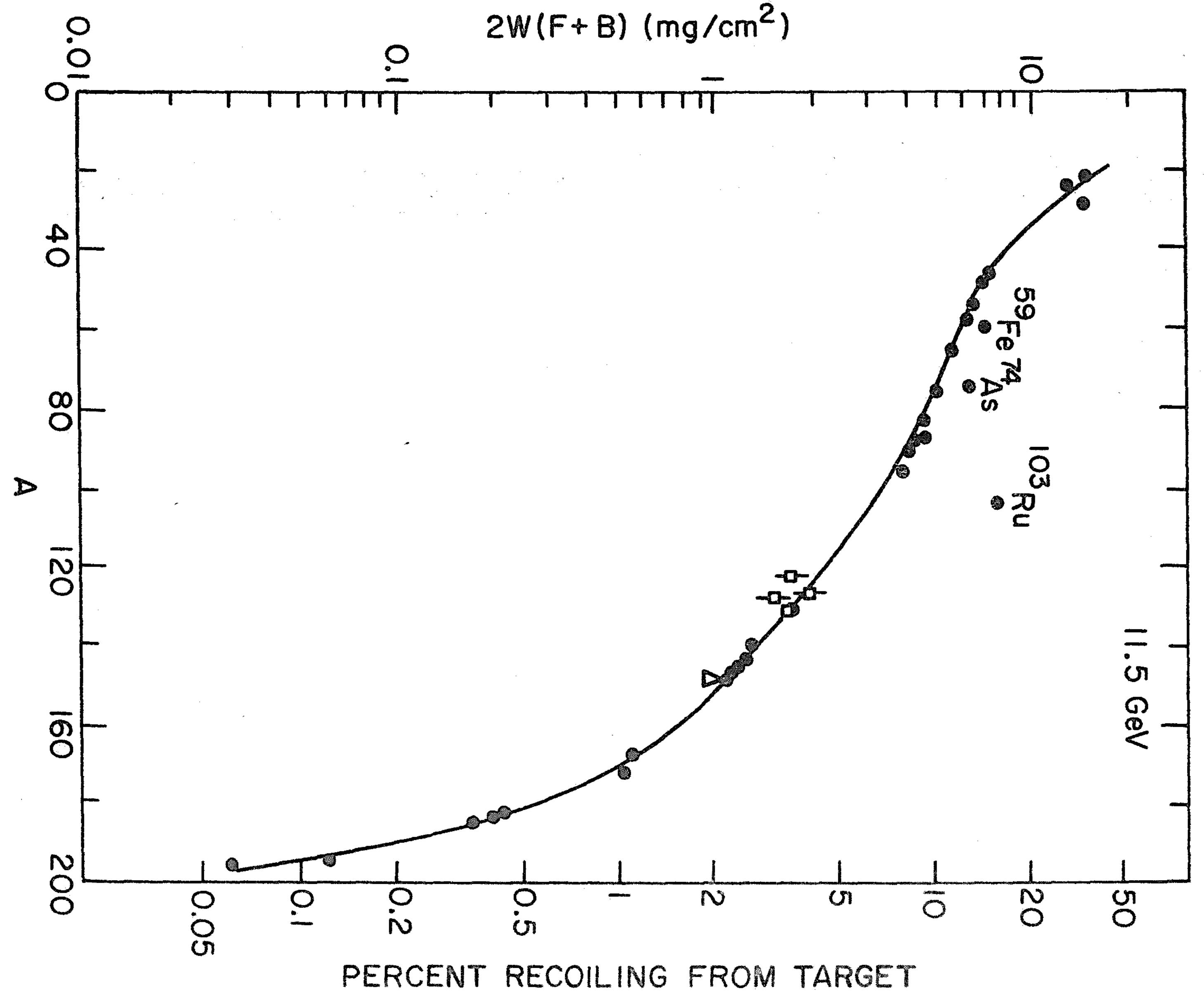
2W(F+B) (mg/cm^2)
0.01
0.1
1
10
0
40
80
120
160
200
A
^{59}Fe
^{74}As
^{103}Ru
11.5 GeV
0.05
0.1
0.2
0.5
1
2
5
10
20
50
PERCENT RECOILING FROM TARGET

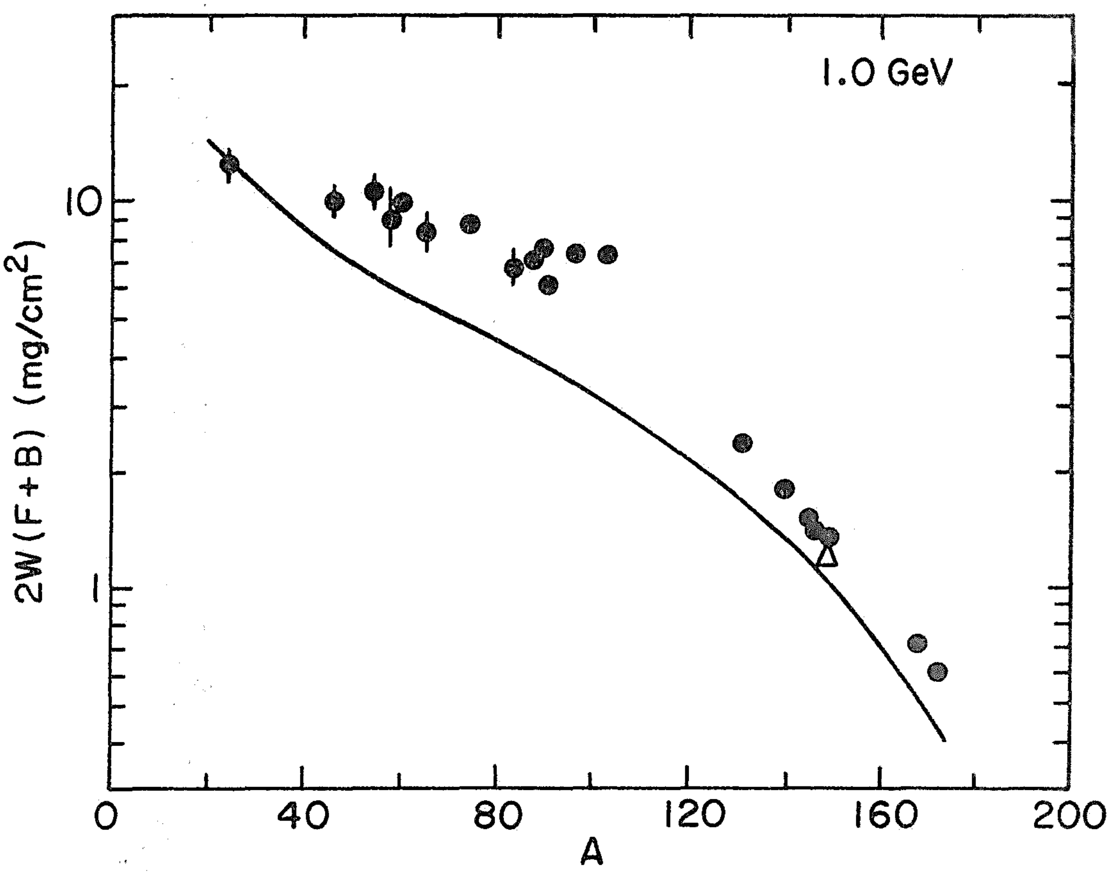
1.0 GeV
2W(F+B) (mg/cm^2)
10
1
0
40
80
120
160
200
A

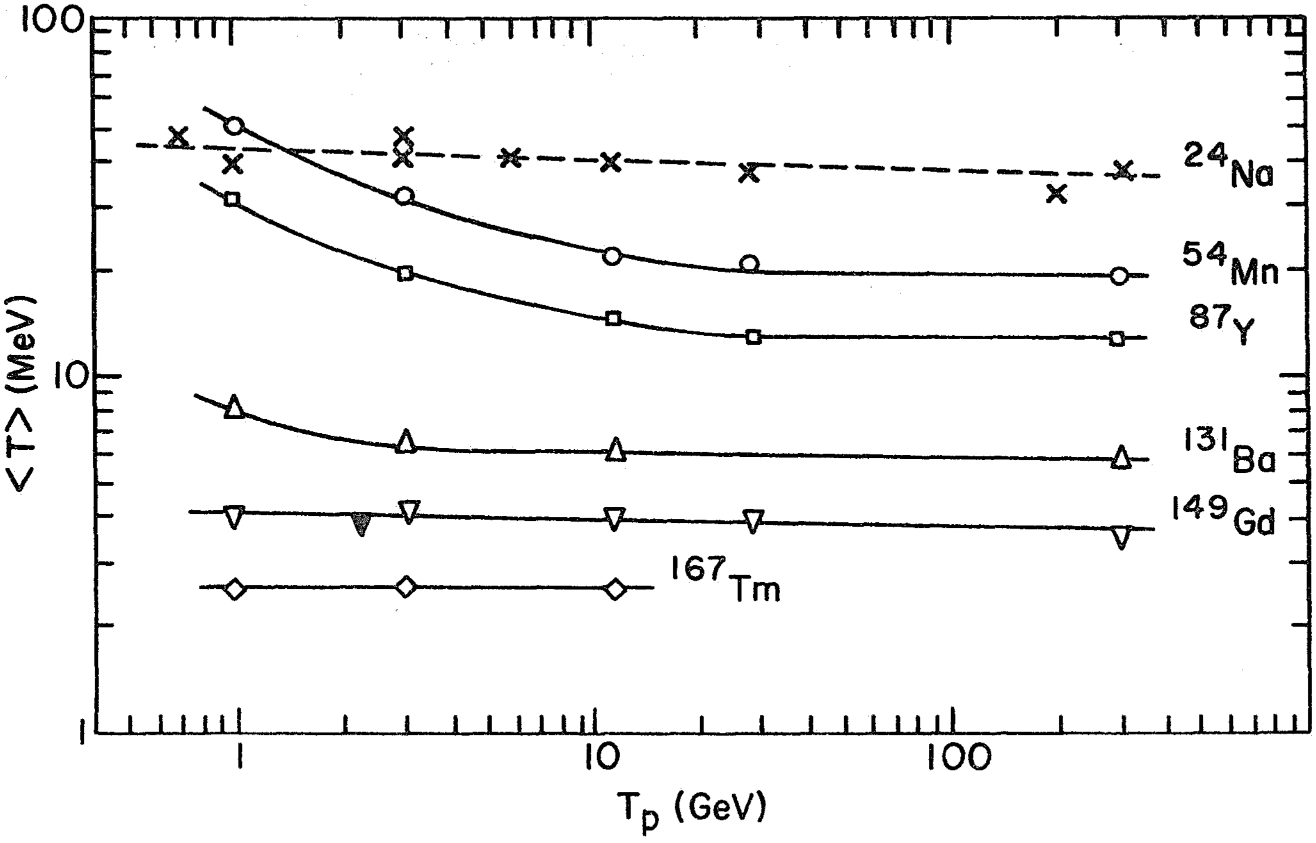

100
10
1
<T> (MeV)
1
10
100
Tp (GeV)
24Na
54Mn
87Y
131Ba
149Gd
167Tm

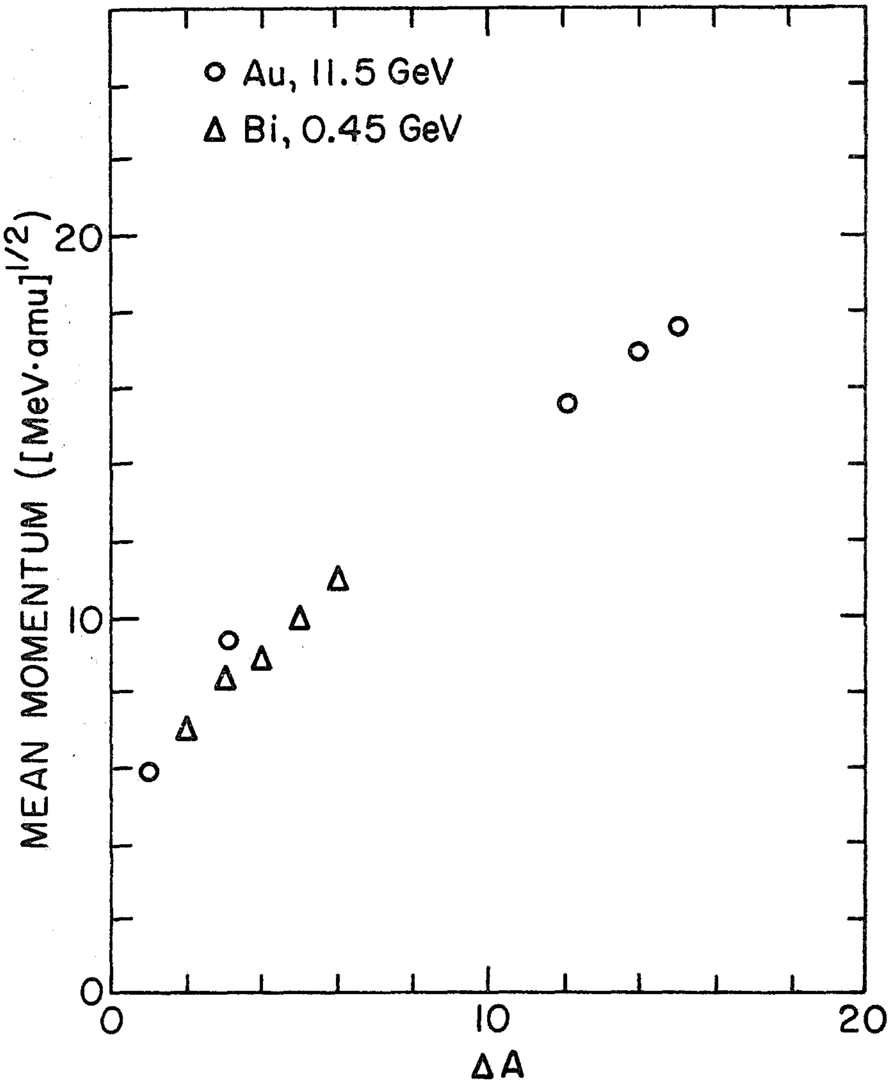

○ Au, 11.5 GeV
Δ Bi, 0.45 GeV
MEAN MOMENTUM ([MeV·amu]$^{1/2}$)
0
10
20
0
10
20
ΔA

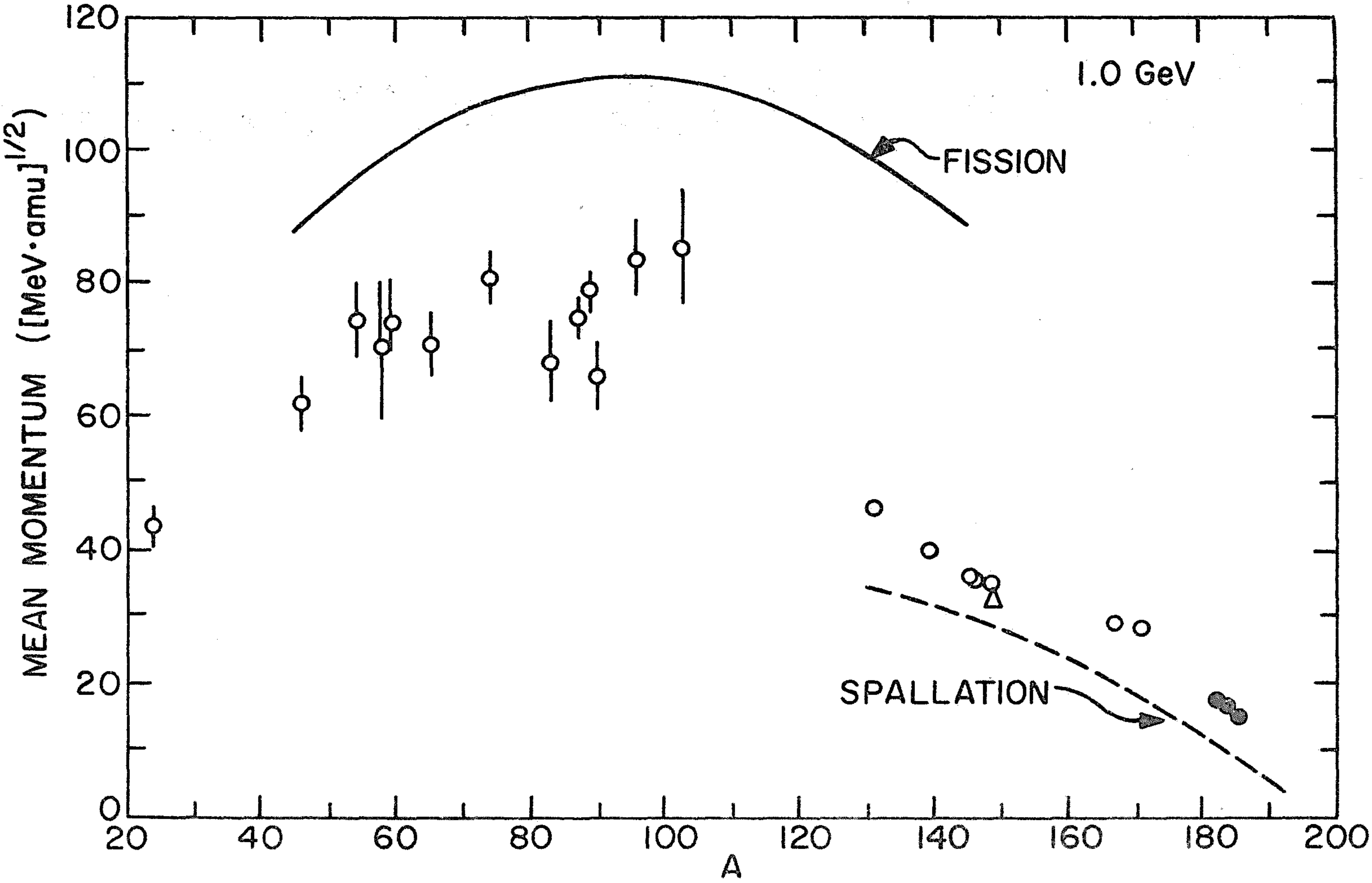
1.0 GeV
FISSION
SPALLATION
MEAN MOMENTUM ([MeV·amu]$^{1/2}$)
A
0
20
40
60
80
100
120
20
40
60
80
100
120
140
160
180
200

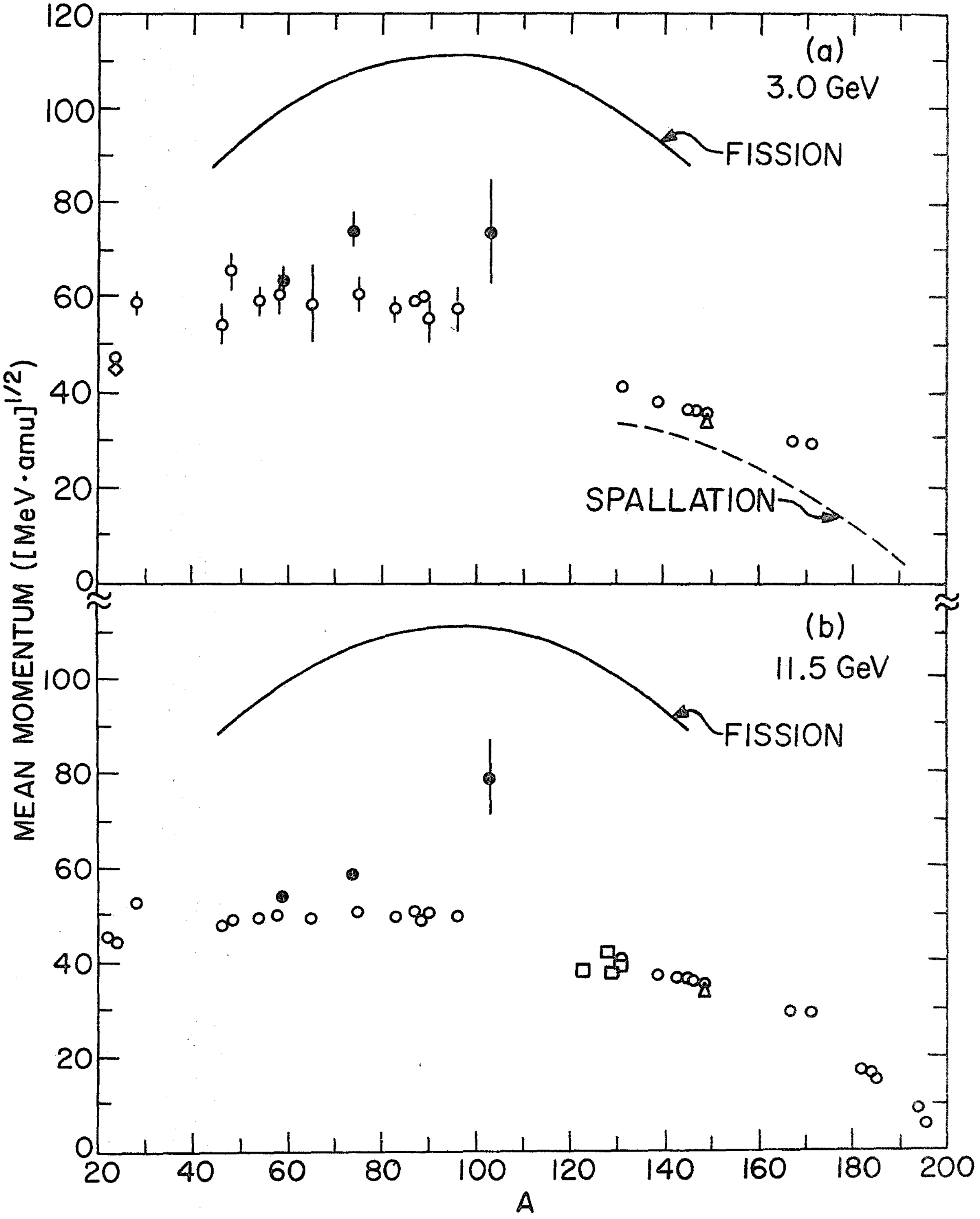
(a)
3.0 GeV
FISSION
SPALLATION
(b)
11.5 GeV
FISSION
MEAN MOMENTUM ([MeV·amu]$^{1/2}$)
A
0
20
40
60
80
100
120
20
40
60
80
100
120
140
160
180
200

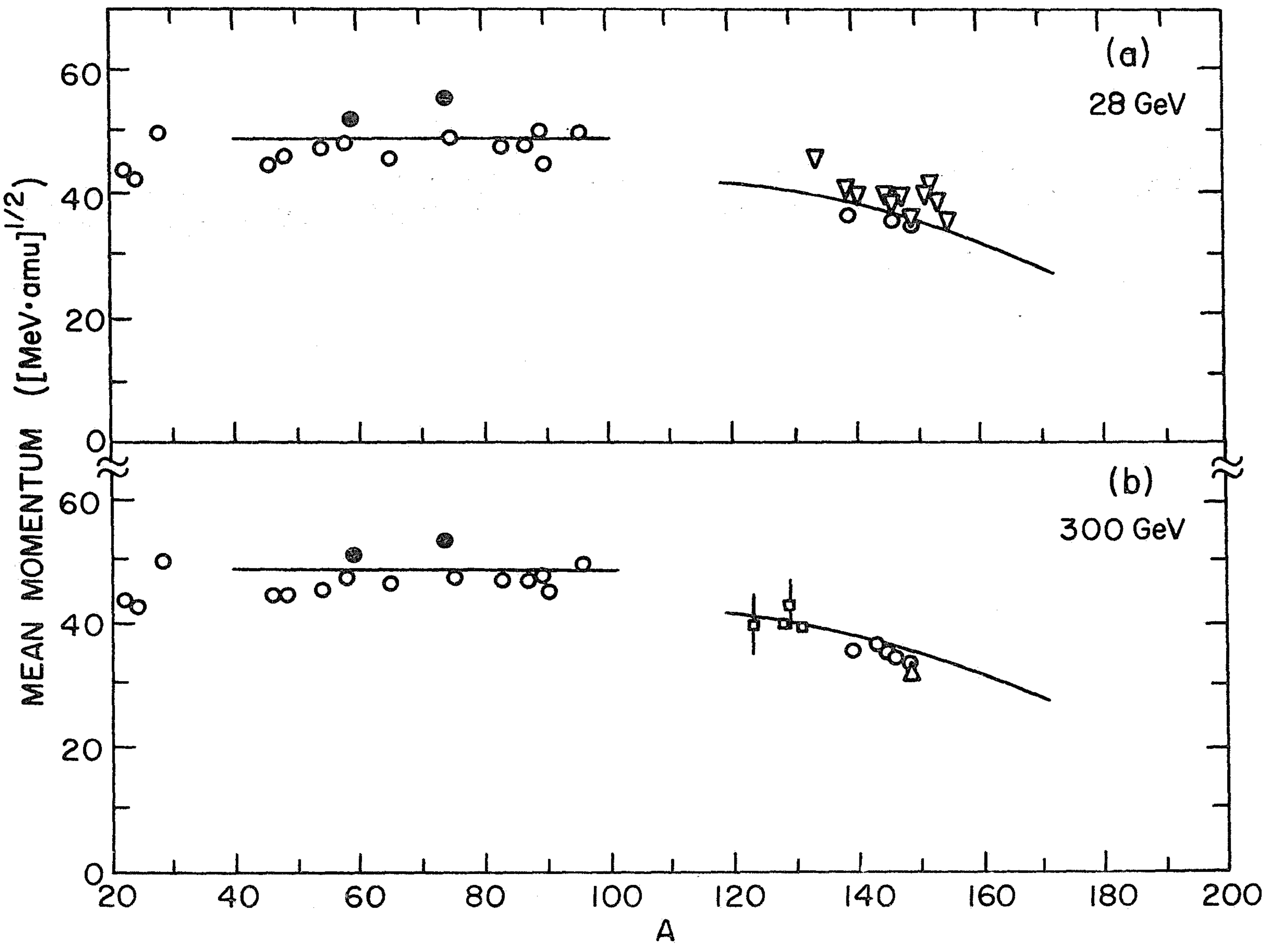
(a)
28 GeV
(b)
300 GeV
MEAN MOMENTUM ([MeV·amu]$^{1/2}$)
0
20
40
60
20
40
60
80
100
120
140
160
180
200
A

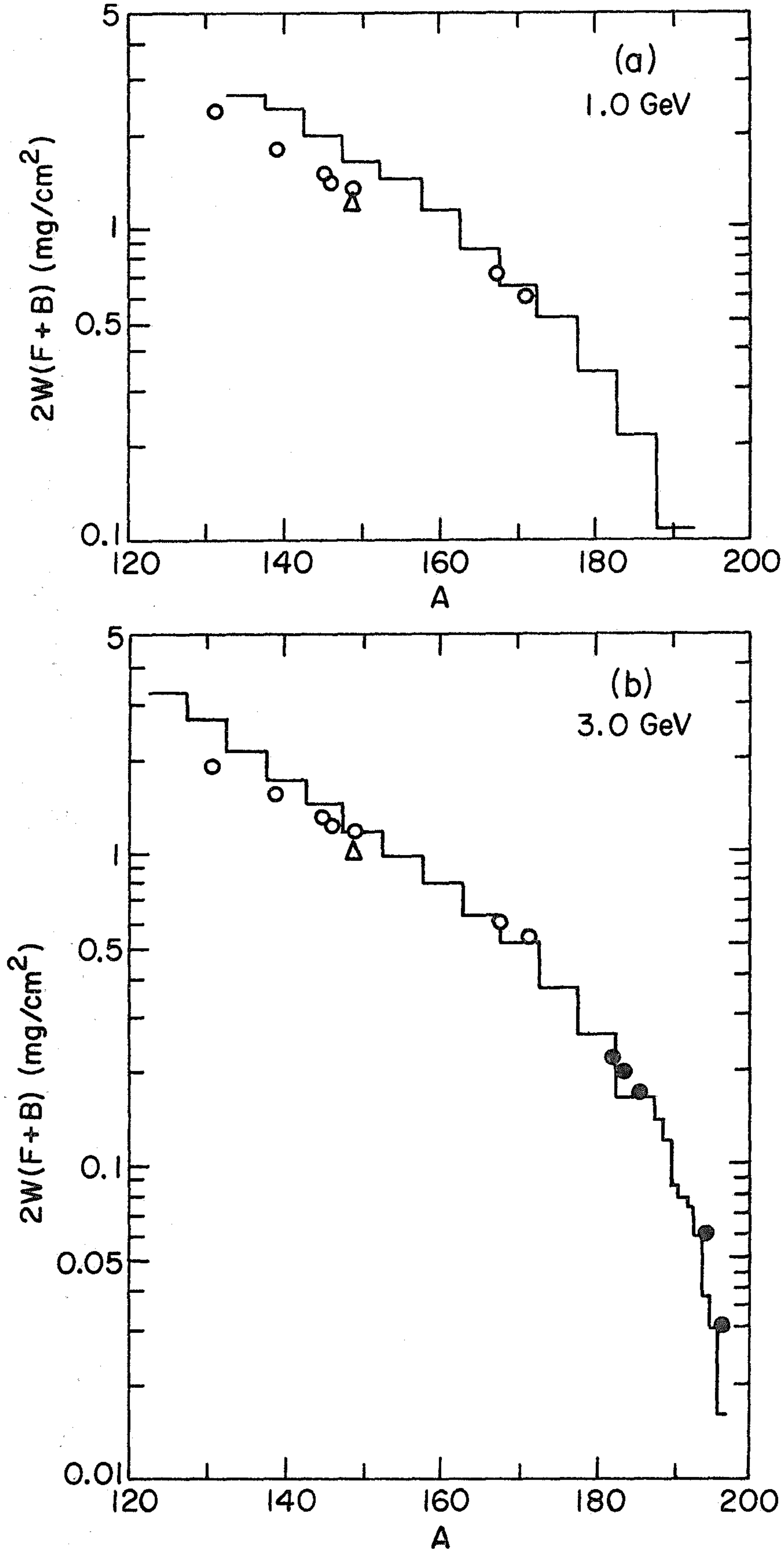
(a)
1.0 GeV
2W(F+B) (mg/cm^2)
5
1
0.5
0.1
120
140
160
180
200
A
(b)
3.0 GeV
2W(F+B) (mg/cm^2)
5
1
0.5
0.1
0.05
0.01
120
140
160
180
200
A

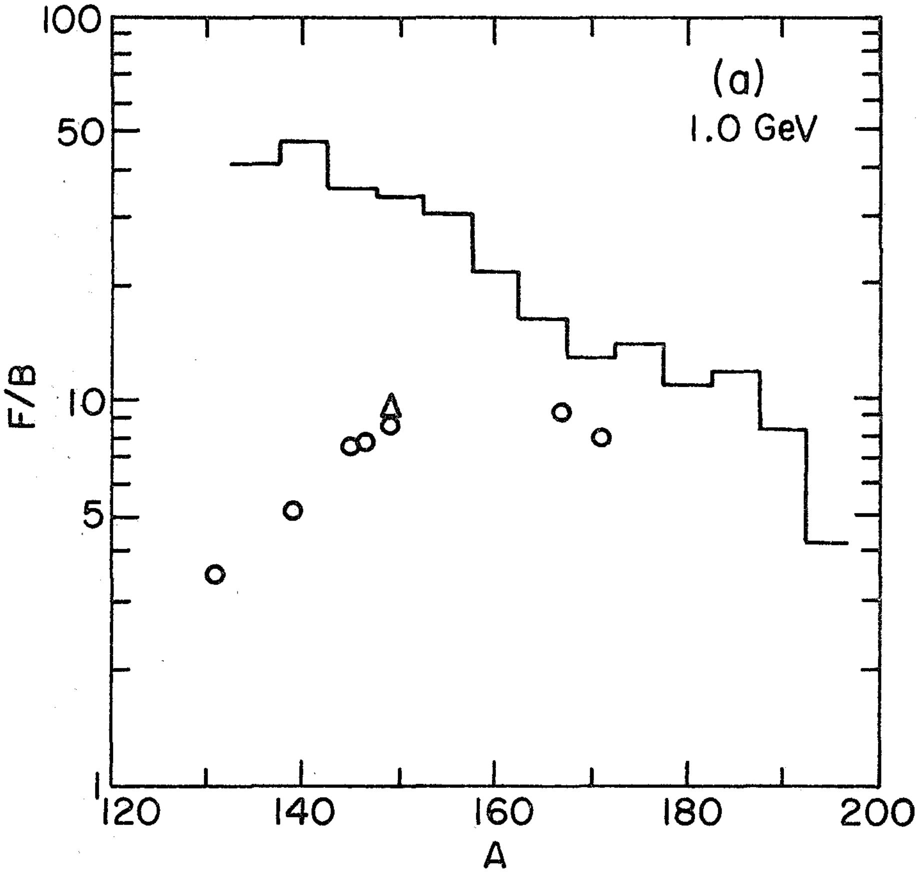
100
50
10
5
1
F/B
(a)
1.0 GeV
A
120
140
160
180
200
A

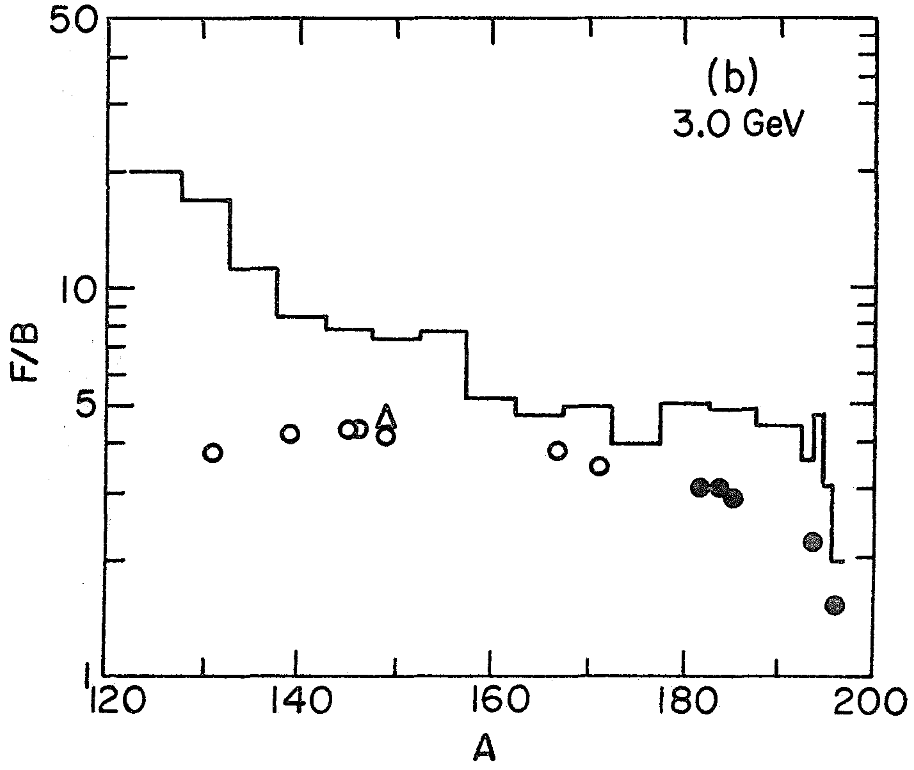
50
10
5
1
F/B
(b)
3.0 GeV
A
120
140
160
180
200
A

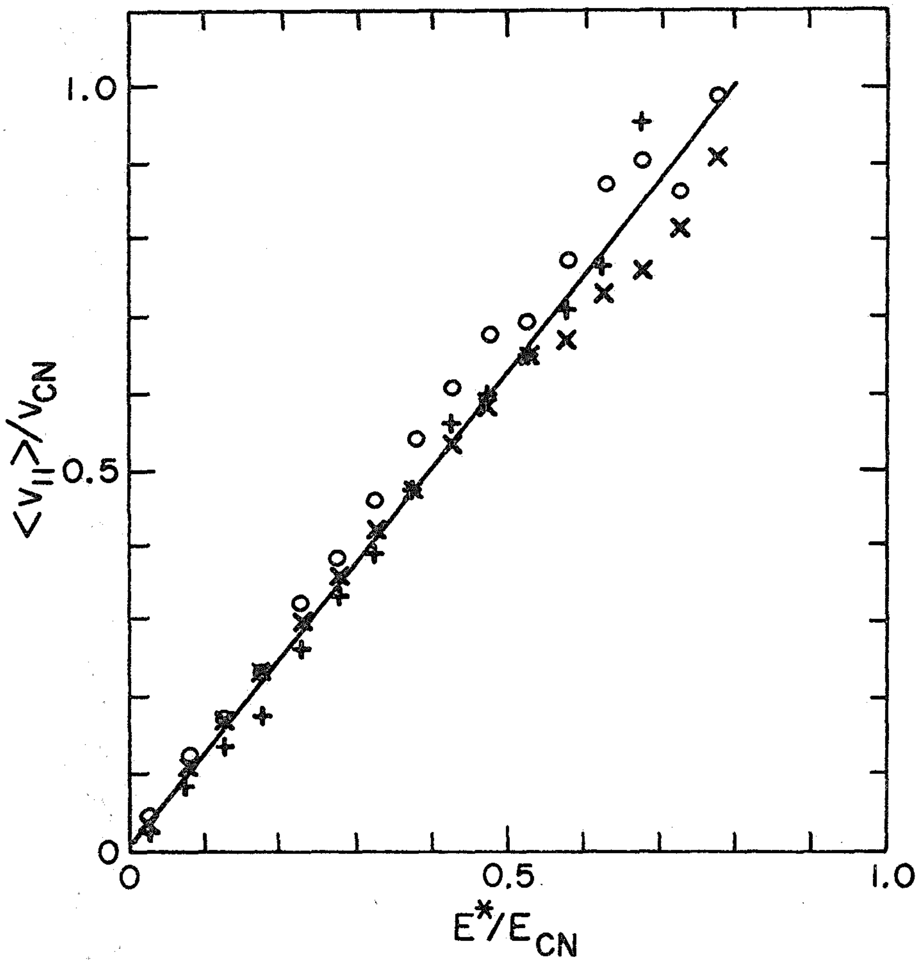

1.0
0.5
0
$\langle v_{\parallel} \rangle / v_{CN}$
0
0.5
1.0
E^{*}/E_{CN}

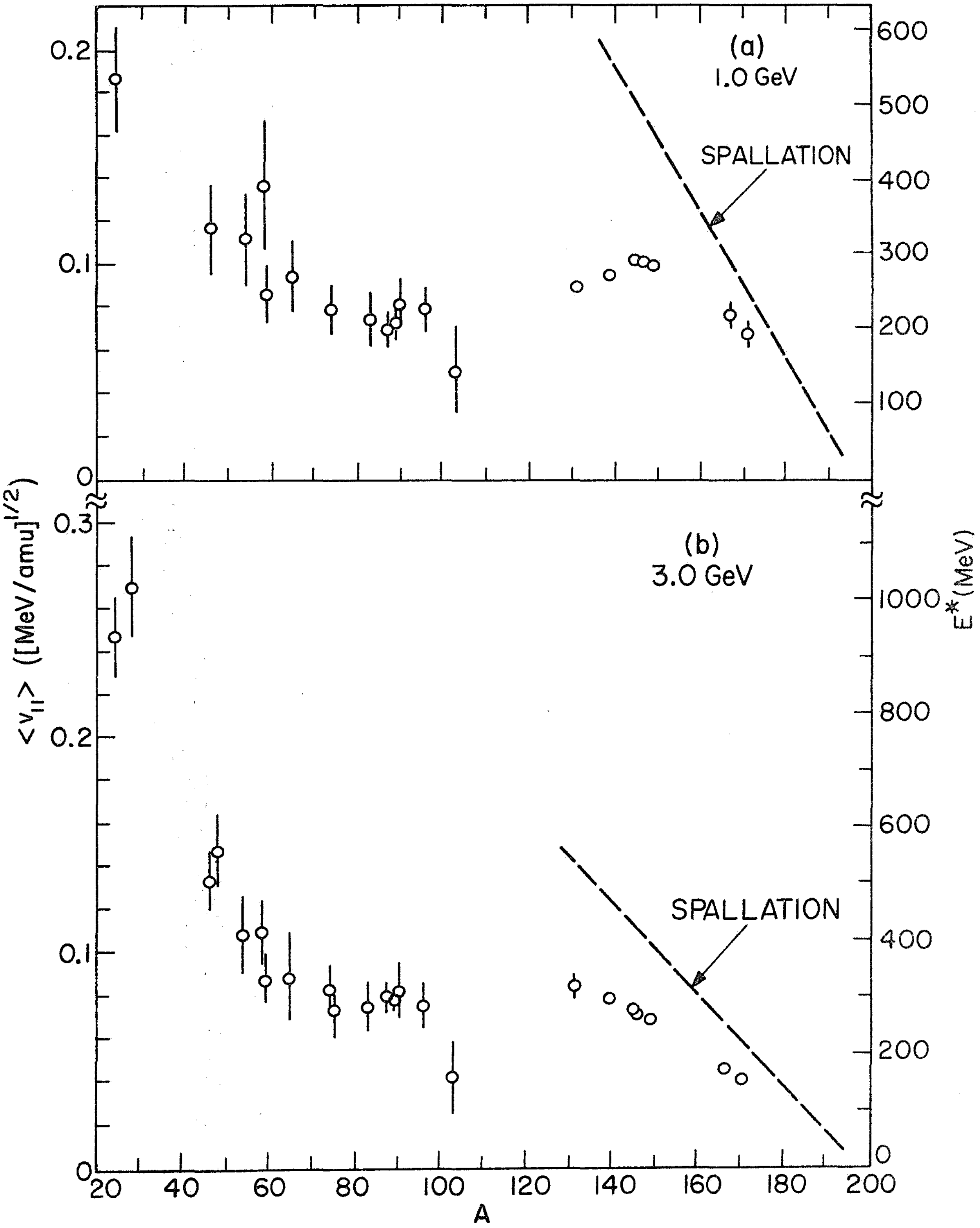
(a)
1.0 GeV
SPALLATION
(b)
3.0 GeV
SPALLATION
$\langle v_{\parallel} \rangle$ ([MeV/amu]$^{1/2}$)
E^* (MeV)
A
0
0.1
0.2
0.3
100
200
300
400
500
600
800
1000
20
40
60
80
100
120
140
160
180
200

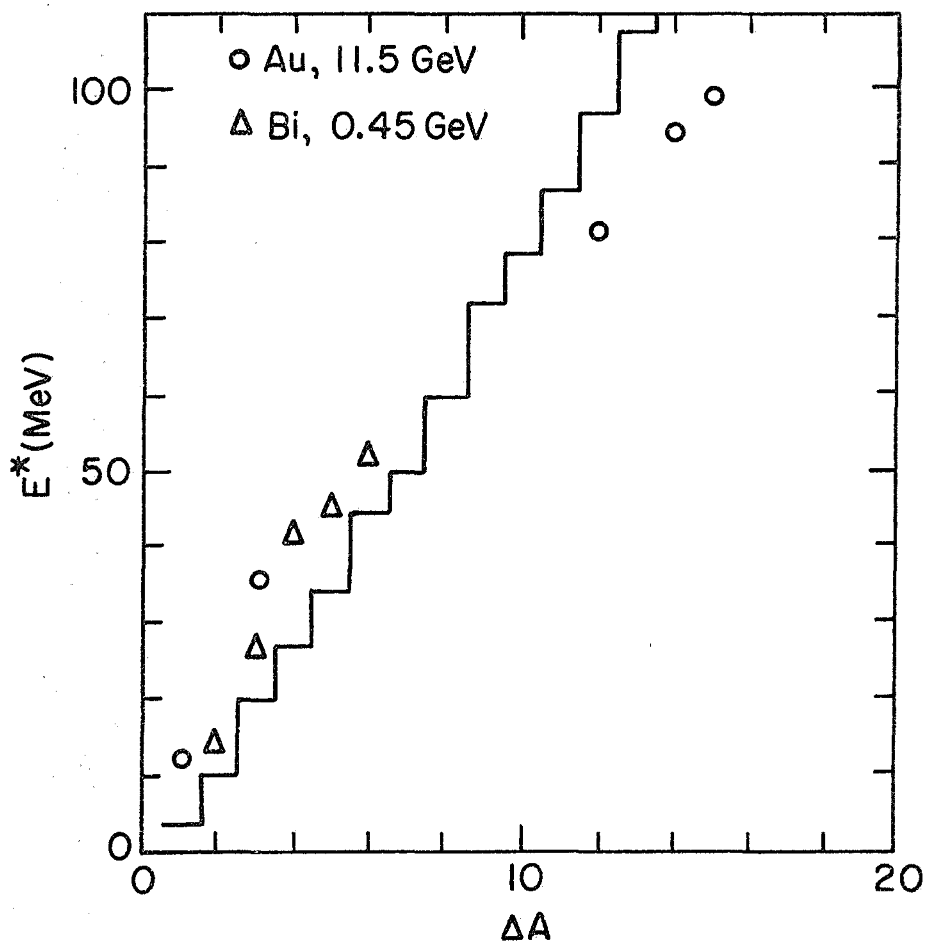
○ Au, 11.5 GeV
Δ Bi, 0.45 GeV
E*(MeV)
100
50
0
0
10
20
ΔA

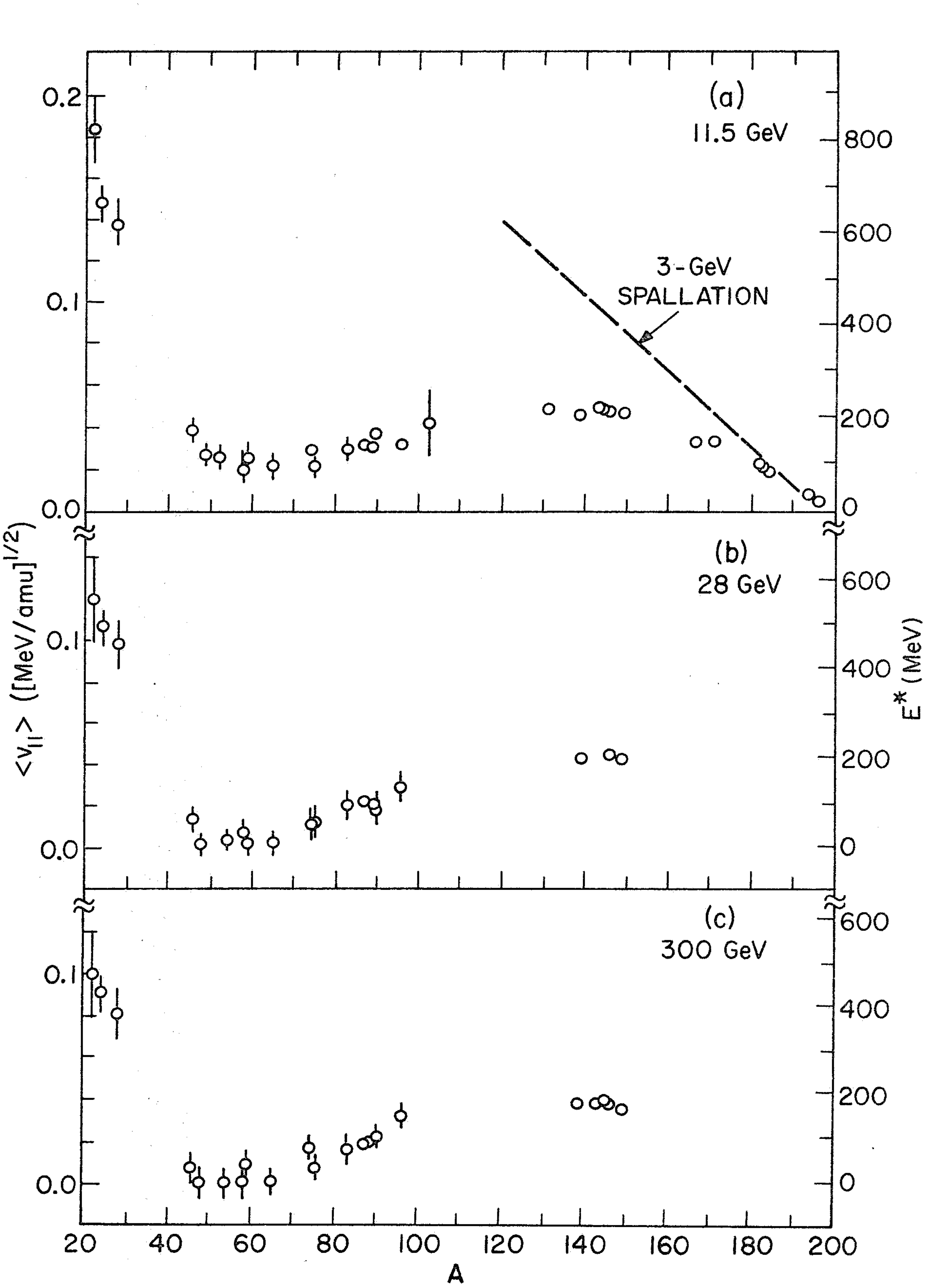
(a)
11.5 GeV
3-GeV
SPALLATION
(b)
28 GeV
(c)
300 GeV
<$v_{\parallel}$> ([MeV/amu]$^{1/2}$)
E* (MeV)
A
0.0
0.1
0.2
0
200
400
600
800
20
40
60
80
100
120
140
160
180
200

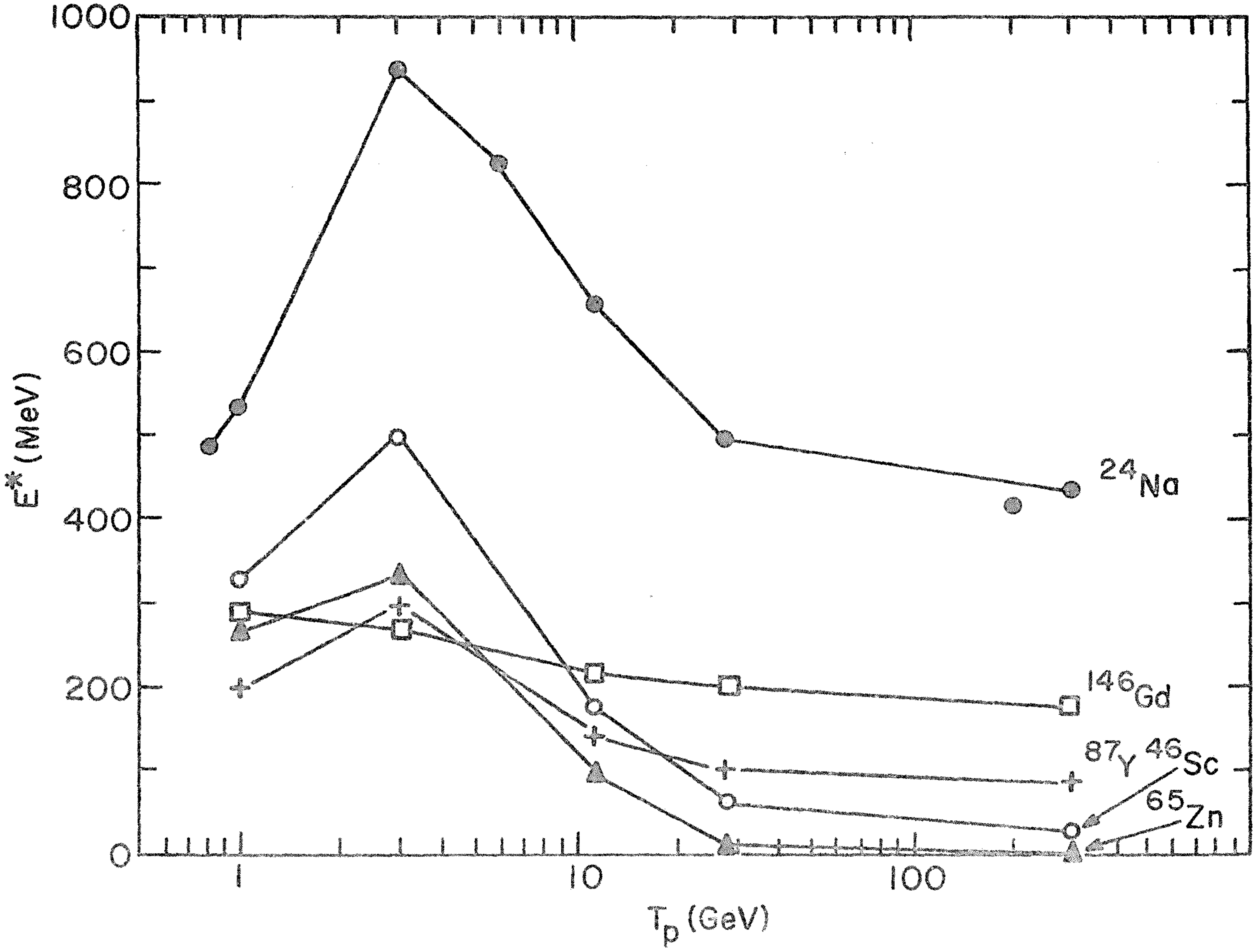
1000
800
600
400
200
0
E* (MeV)
1
10
100
T_p (GeV)
^{24}Na
^{146}Gd
^{87}Y
^{46}Sc
^{65}Zn